SIAM J. SCI. COMPUT.
Vol. 34, No. 3, pp. A1777–A1799




# CERTIFIED REDUCED BASIS METHOD FOR THE ELECTRIC FIELD INTEGRAL EQUATION*

J. S. HESTHAVEN†, B. STAMM‡, AND S. ZHANG†

**Abstract.** In [B. Fares et al., *J. Comput. Phys.*, 230 (2011), pp. 5532–5555], a reduced basis method (RBM) for the electric field integral equation (EFIE) using the boundary element method (BEM) is developed, based on a simplified a posteriori error estimator for the greedy-based snapshot selection. In this paper, we extend this work and propose a certified RBM for the EFIE based on a mathematically rigorous a posteriori estimator. A central difficulty of the certified method is that the intrinsic solution space of the EFIE is $\boldsymbol{H}_{\mathrm{div}}^{-1/2}(\Gamma)$, inducing a relatively complicated norm. Since the measured error consists of the difference between the reduced basis solution and the boundary element solution, which is a member of the discrete boundary element space, we clarify that the intrinsic norm can be replaced by an alternative norm and in this work use the $\boldsymbol{H}(\mathrm{div})$-norm, which is computable and demonstrated to not degrade the quality of the error estimator. A successive constraint method (SCM) for complex matrices is discussed in detail, and numerical tests for the SCM and then the certified RBM confirm the analysis.

**Key words.** basis methods, integral equations, electromagnetics

**AMS subject classifications.** 65R20, 65N15, 78A25, 65R99

**DOI.** 10.1137/110848268

## 1. Introduction.

Many applications related to computational optimization, control, and design require the ability to rapidly and accurately solve parameterized problems many times for different parameter values within a given parametric domain. The reduced basis method (RBM) [10, 12] is an accurate and efficient method for such scenarios allowing a mathematically rigorous error control of the applied model reduction and certification of the accuracy of the output.

In [5], an RBM for parameterized scattering problems in computational electromagnetics for the electric field integral equation (EFIE) [2, 6, 7], discretized using the boundary element method (BEM), is proposed. As is standard for RBMs, a greedy algorithm, based on an a posteriori estimator, is employed to assemble the low-dimensional (reduced basis) approximation space. The quality of these estimates has a direct impact on the approximation properties of the reduced basis. In [5], a simple $L^2$-norm of the residual is used as an error estimator, neglecting the parameter dependence of the involved inf-sup stability constant of the BEM. For the EFIE with the wave-number being a parameter, this constant can be arbitrarily close to zero for some configurations and a constant uniform lower bound may thus lead to very conservative, and in practice useless, error estimates. Thus, to improve the quality of the error estimator and recover a practical certified RBM, we have to design the error estimator to fully incorporate the stability constant.

In [4, 9, 10, 12], the general background for a posteriori error estimators for the

*Submitted to the journal's Methods and Algorithms for Scientific Computing section September 16, 2011; accepted for publication (in revised form) April 3, 2012; published electronically June 28, 2012.

http://www.siam.org/journals/sisc/34-3/84826.html

†Division of Applied Mathematics, Brown University, Providence, RI 02912 (Jan.Hesthaven@Brown.edu, Shun_Zhang@Brown.edu). The work of these authors was supported in part by OSD/AFOSR FA9550-09-1-0613.

‡Department of Mathematics, University of California, Berkeley, Berkeley, CA 94720 (stamm@math.berkeley.edu).

RBM is presented. In these papers, the intrinsic norm of the solution space is used to measure the error. For example, the $H^1$-norm is used for diffusion equations [10] and the $\boldsymbol{H}(\mathrm{curl})$-norm is used for Maxwell's equations [4]. For most problems, this intrinsic norm is the natural choice, as there is often some a priori stability estimates based on these intrinsic norms. In general, the coercivity or the inf-sup stability constant has advantageous properties, making the computation of the coercivity or the inf-sup stability constant in these intrinsic norms more stable.

In this work, we focus on the EFIE, rather than the combined field integral equation (CFIE), which is known for better stability properties in practice, as a first step for a few reasons. First, this work together with [5] is the first of its kind for integral equations and scattering problems. Using the EFIE is reasonably considered as a preliminary step towards a certified RBM for the CFIE. Second, due to the better stability properties of the CFIE with respect to the wave-number, working with the EFIE emerges as a worst case scenario and it is insightful to fully understand this case.

For the EFIE, the a priori estimation is very weak and the existence and uniqueness of the solution are based on the Fredholm alternative theory. There is no a priori estimation for the inf-sup constants for the EFIE, and thus the benefit of using the intrinsic norm is less clear. In addition, the intrinsic solution space is $\boldsymbol{H}_{\mathrm{div}}^{-1/2}(\Gamma)$ [2, 7], a dual space on the surface $\Gamma$. The computation of the $\boldsymbol{H}_{\mathrm{div}}^{-1/2}(\Gamma)$-norm involves the single layer boundary potential integral operator for the Laplacian $-\Delta$ (see, e.g., [13]), which is relatively complicated.

However, as we shall demonstrate in more detail later, we may use other suitable norms. For a particular parameter value, the model reduction error is measured as the difference between the reduced basis solution and the discrete boundary element solution. Both solutions are discrete and can be measured by some simpler and computable norm. In our case, the discrete boundary element space is the lowest-order complex Raviart–Thomas space, which is a conforming subspace of $\boldsymbol{H}_{\mathrm{div}}^{0}(\Gamma)$ equipped with an easily computable $\boldsymbol{H}(\mathrm{div})$-norm. In what follows, we adopt this norm to measure the model reduction error and we shall demonstrate that this does not adversely impact the accuracy of the error estimator.

The corresponding inf-sup stability constants with respect to the $\boldsymbol{H}(\mathrm{div})$-norm are computed by the successive constraint method (SCM) [3, 4, 8]. Different from the presentation in [3], where the real and imaginary parts of a complex matrix are decoupled in the SCM, we improve the algorithm by fully utilizing the properties of Hermitian matrices.

Summarizing, we present a theoretical and computational framework for a *certified* RBM applied to electromagnetic scattering problems described by the EFIE. This work is a succession of [5], where the use of a simple error indicator does not allow the development of rigorous error bounds that certify the error. Our main contributions consist of presenting the complete framework, adapting the SCM to complex matrices, developing problem specific error bounds for the output functional, the radar cross section, and presenting a set of nontrivial numerical examples.

The remainder of this paper is organized as follows. In section 2 we briefly outline the EFIE, the BEM, and the RBM for the EFIE. We develop a certified RBM in section 3, where the error estimator and the SCM for the complex case are presented in detail. Numerical tests are discussed in section 4 to test the SCM and the certified RBM, and section 5 concludes with a few remarks.

**2. EFIE and RBM.** In this section, we review the EFIE and the RBM to offer sufficient context for the remainder. A detailed presentation can be found in [5].

**2.1. Governing equations.** We consider a configuration in three-dimensional space, consisting of an obstacle $D$. The surface of $D$ is denoted by $\Gamma$, and for each point $\boldsymbol{x} \in \Gamma$, we assign a unitary normal vector $\boldsymbol{n}(\boldsymbol{x})$. If $\Gamma$ is a closed surface, we choose the exterior normal.

The obstacle $D$ is situated in a homogeneous medium with vanishing conductivity, free space permittivity $\epsilon_0 = 10^7/(4\pi c^2)\mathrm{F/m}$, and permeability $\mu_0 = 4\pi \times 10^{-7}\mathrm{H/m}$, where $c = 299,792,458$ m/s is the speed of light.

We seek to model the scattering by $D$ of an incident time-harmonic electromagnetic plane wave

$$\boldsymbol{E}^{\mathrm{inc}}(\boldsymbol{x}; k, \hat{\boldsymbol{d}}, \hat{\boldsymbol{p}}) = ik\hat{\boldsymbol{p}}e^{ik\boldsymbol{x}\cdot\hat{\boldsymbol{d}}},$$
$$\boldsymbol{H}^{\mathrm{inc}}(\boldsymbol{x}; k, \hat{\boldsymbol{d}}, \hat{\boldsymbol{p}}) = ik\big(\hat{\boldsymbol{d}}\times\hat{\boldsymbol{p}}\big)e^{ik\boldsymbol{x}\cdot\hat{\boldsymbol{d}}},$$

with $\hat{\boldsymbol{d}} \perp \hat{\boldsymbol{p}}$ and which is parameterized by the wave-number $k \in \mathbb{R}^+$, direction $\hat{\boldsymbol{d}} \in \mathbb{S}^2$, and polarization $\hat{\boldsymbol{p}} \in \mathbb{R}^3$, where $\mathbb{S}^2$ denotes the unit sphere. We identify the polarization vector $\hat{\boldsymbol{p}}$, which is perpendicular to $\hat{\boldsymbol{d}}$, with a vector in $\mathbb{R}^2$ by using a local orthonormal basis that is perpendicular to $\hat{\boldsymbol{d}}$. Then, we denote the set of parameters by $\boldsymbol{\mu} = (k, \hat{\boldsymbol{d}}, \hat{\boldsymbol{p}}) \in \boldsymbol{\mathcal{P}}$ for some parameter domain $\boldsymbol{\mathcal{P}} \subset \mathbb{R}^+ \times \mathbb{S}^2 \times \mathbb{R}^2$. The wavelength of the incident electric and magnetic fields is given by $\lambda = 2\pi/k$.

The total field components $[\boldsymbol{E}, \boldsymbol{H}]$, i.e., the incident and the scattered fields with the latter denoted by $[\boldsymbol{E}^{\mathrm{sca}}, \boldsymbol{H}^{\mathrm{sca}}]$, satisfy the time-harmonic Maxwell equations

$$\mathbf{curl}\, \boldsymbol{E}(\boldsymbol{x}) - i\omega\mu_0\boldsymbol{H}(\boldsymbol{x}) = \boldsymbol{0}, \qquad \mathbf{curl}\, \boldsymbol{H}(\boldsymbol{x}) + i\omega\epsilon_0\boldsymbol{E}(\boldsymbol{x}) = \boldsymbol{0}, \quad \boldsymbol{x} \in \mathbb{R}^3 \setminus \overline{D}, \tag{2.1}$$

and the Silver–Müller radiation condition

$$\lim_{|\boldsymbol{x}|\to\infty} [\boldsymbol{H}(\boldsymbol{x})\times\boldsymbol{x} - |\boldsymbol{x}|\boldsymbol{E}(\boldsymbol{x})] = \boldsymbol{0}. \tag{2.2}$$

We assume that the obstacle $D$ is perfectly conducting and hence the tangential component of the total electric field $\boldsymbol{E}$ vanishes on the surface of $D$, yielding the boundary condition

$$\boldsymbol{n}(\boldsymbol{x})\times\boldsymbol{E}^{\mathrm{sca}}(\boldsymbol{x}) = -\boldsymbol{n}(\boldsymbol{x})\times\boldsymbol{E}^{\mathrm{inc}}(\boldsymbol{x}), \qquad \boldsymbol{x} \in \Gamma. \tag{2.3}$$

Using the Stratton–Chu representation formula, the scattered electric and the magnetic fields can be represented by

$$\boldsymbol{E}^{\mathrm{sca}}(\boldsymbol{x}) = ikZ \int_\Gamma \Big[\mathcal{G}(r;k)\boldsymbol{u}(\boldsymbol{y}) + \tfrac{1}{k^2}\mathbf{grad}_{\boldsymbol{x}}\mathcal{G}(r;k)\mathrm{div}_{\Gamma,y}\boldsymbol{u}(\boldsymbol{y})\Big]\, d\boldsymbol{y},$$
$$\boldsymbol{H}^{\mathrm{sca}}(\boldsymbol{x}) = -\tfrac{i}{kZ}\mathbf{curl}\, \boldsymbol{E}^{\mathrm{sca}}(\boldsymbol{x}),$$

where $Z = \sqrt{(\mu_0/\epsilon_0)}$ is the free space impedance and $\mathcal{G}$ is the fundamental solution of the Helmholtz operator defined by

$$\mathcal{G}(r,k) = \frac{e^{ikr}}{4\pi r}, \qquad r = |\boldsymbol{x} - \boldsymbol{y}|.$$

Invoking the boundary condition for $\boldsymbol{E}$ yields the EFIE

$$\mathbf{T}[\boldsymbol{u}(\boldsymbol{x};\boldsymbol{\mu});\boldsymbol{\mu}] = \mathbf{f}[\boldsymbol{x};\boldsymbol{\mu}], \tag{2.4}$$

where

$$\mathbf{T}[\boldsymbol{u}(\boldsymbol{x};\boldsymbol{\mu});\boldsymbol{\mu}] = ikZ\,\gamma_t\left(\int_\Gamma \left[\mathcal{G}(r;k)\boldsymbol{u}(\boldsymbol{y}) + \tfrac{1}{k^2}\mathbf{grad}_{\boldsymbol{x}}\mathcal{G}(r;k)\mathrm{div}_{\Gamma,y}\boldsymbol{u}(\boldsymbol{y})\right] d\boldsymbol{y}\right),$$
$$\mathbf{f}[\boldsymbol{x};\boldsymbol{\mu}] = -\gamma_t\left(\boldsymbol{E}^{\mathrm{inc}}(\boldsymbol{x};\boldsymbol{\mu})\right),$$

with $\gamma_t(\boldsymbol{u}) = \boldsymbol{n}\times(\boldsymbol{u}\times\boldsymbol{n})$ on $\Gamma$. The EFIE can be cast in terms of a variational problem: for a given parameter value $\boldsymbol{\mu}\in\boldsymbol{\mathcal{P}}$, find $\boldsymbol{u}(\boldsymbol{\mu})\in\boldsymbol{X} := \boldsymbol{H}^{-\frac{1}{2}}_{\mathrm{div}}(\Gamma)$ such that

$$a[\boldsymbol{u}(\boldsymbol{\mu}),\boldsymbol{v};\boldsymbol{\mu}] = f[\boldsymbol{v};\boldsymbol{\mu}] \tag{2.5}$$

for all $\boldsymbol{v}\in\boldsymbol{X}$. The sesquilinear and linear forms are given by

$$\begin{aligned} a[\boldsymbol{u},\boldsymbol{v};\boldsymbol{\mu}] &= ikZ\int_{\Gamma\times\Gamma}\mathcal{G}(r;k)\boldsymbol{u}(\boldsymbol{y})\cdot\overline{\boldsymbol{v}(\boldsymbol{x})}\,d\boldsymbol{y}\,d\boldsymbol{x} \\ &\quad - \tfrac{iZ}{k}\int_{\Gamma\times\Gamma}\mathcal{G}(r;k)\mathrm{div}_{\Gamma,y}\boldsymbol{u}(\boldsymbol{y})\mathrm{div}_{\Gamma,x}\overline{\boldsymbol{v}(\boldsymbol{x})}\,d\boldsymbol{y}\,d\boldsymbol{x}, \\ f[\boldsymbol{v};\boldsymbol{\mu}] &= -\int_\Gamma \boldsymbol{E}^{\mathrm{inc}}(\boldsymbol{x};\boldsymbol{\mu})\cdot\overline{\boldsymbol{v}(\boldsymbol{x})}\,d\boldsymbol{x}. \end{aligned}$$

Here and in the following we use $\boldsymbol{u}$ instead of $\boldsymbol{u}(\boldsymbol{\mu})$ for the sake of simple presentation unless clarification is needed. Note that projecting $\boldsymbol{E}^{\mathrm{inc}}(\boldsymbol{x};\boldsymbol{\mu})$ onto the surface $\Gamma$ is no longer necessary since $\boldsymbol{v}$ is a tangential function.

Let $\mathcal{T}_h$ be a family of shape-regular triangulations decomposing $\Gamma$ into flat triangles. By $\boldsymbol{RT}_0(T)$ we denote the local Raviart–Thomas space on $\Gamma$ of complex-valued functions on $T\in\mathcal{T}_h$ defined by (cf. [11])

$$\boldsymbol{RT}_0(T) := \left\{\boldsymbol{v}_h(\boldsymbol{x}) = \boldsymbol{\alpha}+\beta\boldsymbol{x}\,\middle|\,\boldsymbol{\alpha}\in\mathbb{C}^2,\beta\in\mathbb{C},\boldsymbol{x}\in T\right\}.$$

On a global level, the Raviart–Thomas space is defined by

$$\boldsymbol{X}_h := \left\{\boldsymbol{v}_h\in\boldsymbol{H}^0_{\mathrm{div}}(\Gamma)\,\middle|\,\boldsymbol{v}_h|_T\in\boldsymbol{RT}_0(T)\quad\forall T\in\mathcal{T}_h\right\}, \tag{2.6}$$

where $\boldsymbol{H}^0_{\mathrm{div}}(\Gamma)$ is defined in a standard manner:

$$\boldsymbol{H}^0_{\mathrm{div}}(\Gamma) := \left\{\boldsymbol{v}\in\boldsymbol{L}^2_t(\Gamma)\,\middle|\,\mathrm{div}_\Gamma\boldsymbol{v}\in L^2(\Gamma)\right\}.$$

Observe that the approximation space is conforming, i.e., $\boldsymbol{X}_h\subset\boldsymbol{H}^0_{\mathrm{div}}(\Gamma)\subset\boldsymbol{H}^{-1/2}_{\mathrm{div}}(\Gamma)$.

The corresponding BEM consists of seeking, for any given parameter value $\boldsymbol{\mu}\in\boldsymbol{\mathcal{P}}$, the discrete solution $\boldsymbol{u}_h(\boldsymbol{\mu})\in\boldsymbol{X}_h$ such that

$$a[\boldsymbol{u}_h(\boldsymbol{\mu}),\boldsymbol{v}_h;\boldsymbol{\mu}] = f[\boldsymbol{v}_h;\boldsymbol{\mu}] \tag{2.7}$$

for all $\boldsymbol{v}_h\in\boldsymbol{X}_h$.

For different configurations defined by a particular value of the parameter $\boldsymbol{\mu} = (k,\hat{\boldsymbol{d}},\hat{\boldsymbol{p}})\in\boldsymbol{\mathcal{P}}$, we are interested in obtaining the radar cross section (RCS) of $D$, measured by a receiver situated in the direction $\hat{\boldsymbol{d}}_0\in\mathbb{S}^2$. We denote the set of parameters for the output functional by $\boldsymbol{\mu}_s\in\boldsymbol{\mathcal{P}_s}$ for some parameter domain $\boldsymbol{\mathcal{P}_s}\subset\mathbb{R}^+\times\mathbb{S}^2$, containing the wave-number $k$ and some directional unit vector $\hat{\boldsymbol{d}}_0\in\mathbb{S}^2$.

The RCS is an indication of the directional far field associated with a scatterer $D$ subject to illumination by a plane monochromatic wave. It is a functional of the electric current $\boldsymbol{u}(\boldsymbol{\mu})$ on the surface and is defined by

$$\mathrm{rcs}[\boldsymbol{u}(\boldsymbol{\mu});\boldsymbol{\mu},\boldsymbol{\mu}_s] := 10\log_{10}\left(4\pi\frac{|\boldsymbol{s}_\infty[\boldsymbol{u}(\boldsymbol{\mu});\boldsymbol{\mu}_s]|^2}{|\boldsymbol{E}^{\mathrm{inc}}(\boldsymbol{\mu})|^2}\right),$$

where $\boldsymbol{s}_\infty$ is a linear functional of $\boldsymbol{u}(\boldsymbol{\mu})$ given by

$$\boldsymbol{s}_\infty[\boldsymbol{u}(\boldsymbol{\mu});\boldsymbol{\mu}_s] := \frac{ikZ}{4\pi}\int_\Gamma \hat{\boldsymbol{d}}_0\times(\boldsymbol{u}(\boldsymbol{x};\boldsymbol{\mu})\times\hat{\boldsymbol{d}}_0)e^{ik\boldsymbol{x}\cdot\hat{\boldsymbol{d}}_0}\,d\boldsymbol{x}.$$

The RCS represents the energy of the total electric field $\boldsymbol{E}$ at infinity in the direction $\hat{\boldsymbol{d}}_0$.

**2.2. Introduction to the RBM.** For parameterized scattering problems, we are interested in a fast evaluation of the following input-output procedure:

$$\boldsymbol{\mu}\in\boldsymbol{\mathcal{P}} \quad\longrightarrow\quad \text{solve: } L_h[\boldsymbol{u}_h(\boldsymbol{\mu});\boldsymbol{\mu}]=0 \quad\longrightarrow\quad \text{rcs}[\boldsymbol{u}_h(\boldsymbol{\mu});\boldsymbol{\mu},\boldsymbol{\mu}_s], \tag{2.8}$$

where solving $L_h[\boldsymbol{u}_h(\boldsymbol{\mu});\boldsymbol{\mu}]=0$ schematically represents solving problem (2.7). We refer to this procedure as the *truth solver*.

We consider problems where the output functional $\text{rcs}\,[\boldsymbol{u}_h(\boldsymbol{\mu});\boldsymbol{\mu},\boldsymbol{\mu}_s]$ needs to be computed for many different parameter values $\boldsymbol{\mu}$. In this case, solving the full boundary element problem for each new parameter value is not a viable option. The RBM is an algorithmic completion of the BEM to rapidly solve

$$\boldsymbol{\mu}\in\boldsymbol{\mathcal{P}} \quad\longrightarrow\quad \text{solve: } L_N[\boldsymbol{u}_N(\boldsymbol{\mu});\boldsymbol{\mu}]=0 \quad\longrightarrow\quad \text{rcs}[\boldsymbol{u}_N(\boldsymbol{\mu});\boldsymbol{\mu},\boldsymbol{\mu}_s]. \tag{2.9}$$

The reduced basis space approximates the discrete space

$$\boldsymbol{X}_N \approx \{\boldsymbol{u}_h(\boldsymbol{\mu})\,:\,\boldsymbol{\mu}\in\boldsymbol{\mathcal{P}}\},$$

and accuracy of the scheme is controlled by the quality of this approximation. We denote the dimension of $\boldsymbol{X}_N$ by $N$ and the dimension of the boundary element space $\boldsymbol{X}_h$ by $\mathcal{N}$. Solving $L_N[\boldsymbol{u}_N(\boldsymbol{\mu});\boldsymbol{\mu}]=0$ consists of the following: for any given parameter value $\boldsymbol{\mu}\in\boldsymbol{\mathcal{P}}$, find the discrete solution $\boldsymbol{u}_N(\boldsymbol{\mu})\in\boldsymbol{X}_N$ such that

$$a[\boldsymbol{u}_N(\boldsymbol{\mu}),\boldsymbol{v}_N;\boldsymbol{\mu}] = f[\boldsymbol{v}_N;\boldsymbol{\mu}] \tag{2.10}$$

for all $\boldsymbol{v}_N\in\boldsymbol{X}_N$. The complexity of this problem depends on $N$ and is independent of $\mathcal{N}$. Empirically, for the problems under consideration one can observe that $N\ll\mathcal{N}$, making it clear that there is a substantial advantage in solving the reduced basis problem $L_N[\boldsymbol{u}_N(\boldsymbol{\mu});\boldsymbol{\mu}]=0$, which is expected to be much faster than solving the full boundary element problem. However, the remaining questions are the following:

- How does one find basis functions for $\boldsymbol{X}_N$?
- How does one solve (2.10) efficiently?

The common approach for RBMs is to build $\boldsymbol{X}_N$ as the span of solution to (2.7) for particular parameter values (called *snapshots*), i.e.,

$$\boldsymbol{X}_N = \text{span}\{\boldsymbol{u}_h(\boldsymbol{\mu}_1),\ldots,\boldsymbol{u}_h(\boldsymbol{\mu}_N)\},$$

where $\boldsymbol{\mu}_1,\ldots,\boldsymbol{\mu}_N$ are selectively chosen parameters. Those sample points are selected using a greedy algorithm [12] to optimize cost and accuracy. Given an error indicator $\eta(\boldsymbol{\mu})\approx\|\boldsymbol{u}_h(\boldsymbol{\mu})-\boldsymbol{u}_N(\boldsymbol{\mu})\|_{\boldsymbol{X}_h}$ to quantify the error of the reduced basis approximation of (2.10) with respect to the boundary element solution (2.7) (the *truth solution*) and

measured in a given norm $\|\cdot\|_{\boldsymbol{X}_h}$, we proceed as follows:

0: Pick arbitrarily $\boldsymbol{\mu}_1 \in \boldsymbol{\mathcal{P}}$, set $N = 1$ and $W_0 = \emptyset$.

1: Solve $L_h(\boldsymbol{u}_h(\boldsymbol{\mu}_N); \boldsymbol{\mu}_N) = 0$, set $W_N = \text{span}\{W_{N-1}, \boldsymbol{u}_h(\boldsymbol{\mu}_N)\}$.

2: Consider the procedure

$$\boldsymbol{\mu} \in \boldsymbol{\mathcal{P}} \quad \longrightarrow \quad \text{solve: } L_N(\boldsymbol{u}_N(\boldsymbol{\mu}); \boldsymbol{\mu}) = 0 \quad \longrightarrow \quad \eta(\boldsymbol{\mu})$$

and find $\boldsymbol{\mu}_{N+1} = \text{argmax}_{\boldsymbol{\mu}\in\boldsymbol{\mathcal{P}}}\eta(\boldsymbol{\mu})$.

3: Set $N := N + 1$ and go to 1.

This procedure is applied until $\max_{\boldsymbol{\mu}\in\boldsymbol{\mathcal{P}}} \eta(\boldsymbol{\mu})$ is small enough or a maximum of iterations is attained. In this manner, an $N$-dimensional reduced basis space is constructed by solving $N$ boundary element problems. In addition, we obtain a hierarchical basis.

In practical computations, one often replaces the parameter domain $\boldsymbol{\mathcal{P}}$ by a discrete and fine enough point set $\Xi \subset \boldsymbol{\mathcal{P}}$. That is, $\text{argmax}_{\boldsymbol{\mu}\in\Xi}\eta(\boldsymbol{\mu})$ is computed instead of $\text{argmax}_{\boldsymbol{\mu}\in\boldsymbol{\mathcal{P}}}\eta(\boldsymbol{\mu})$.

In order to select only the necessary modes, it is important that the error estimate $\eta(\boldsymbol{\mu})$ be as accurate as possible. In addition, if the estimate is such that

$$\eta(\boldsymbol{\mu}) \geq \|\boldsymbol{u}_h(\boldsymbol{\mu}) - \boldsymbol{u}_N(\boldsymbol{\mu})\|_{\boldsymbol{X}_h}$$

and the computable error estimate guarantees that $\eta(\boldsymbol{\mu}) \leq \texttt{Tol}$ for all parameter values, then a minimal error tolerance of $\|\boldsymbol{u}_h(\boldsymbol{\mu}) - \boldsymbol{u}_N(\boldsymbol{\mu})\|_{\boldsymbol{X}_h} \leq \texttt{Tol}$ can be *certified*. For more details, see section 3.1.

The second point requiring attention is how to solve $L_N[\boldsymbol{u}_N(\boldsymbol{\mu}); \boldsymbol{\mu}] = 0$, i.e., (2.10), efficiently. As stated earlier, problem (2.10) can be written as an $N$-dimensional linear system

$$\mathbf{A}(\boldsymbol{\mu})\, \boldsymbol{U}_N(\boldsymbol{\mu}) = \mathbf{F}(\boldsymbol{\mu}),$$

where $\mathbf{A}(\boldsymbol{\mu})$ is the matrix corresponding to the sesquilinear form $a[\cdot, \cdot; \boldsymbol{\mu}]$ and $\mathbf{F}(\boldsymbol{\mu})$ is the vector corresponding to the linear form $f[\cdot; \boldsymbol{\mu}]$, whereas $\boldsymbol{U}_N(\boldsymbol{\mu})$ is the solution vector, i.e., the representation of $\boldsymbol{u}_N(\boldsymbol{\mu})$ in a chosen basis of $\boldsymbol{X}_N$. This is an $N$-dimensional system. Thus, solving it does not depend on the dimension $\mathcal{N}$ of the underlying boundary element space $\boldsymbol{X}_h$. However, assembling the matrix $\mathbf{A}(\boldsymbol{\mu})$ depends on $\mathcal{N}$. Since one is interested in computing the reduced basis solution for many different parameter values, it is important to satisfy the following affine decomposition property:

$$a[\boldsymbol{u}, \boldsymbol{v}; \boldsymbol{\mu}] = \sum_{q=1}^{Q_{\mathtt{a}}} \theta_{\mathtt{a}}^q(\boldsymbol{\mu})\, a^q[\boldsymbol{u}, \boldsymbol{v}], \tag{2.11}$$

$$f[\boldsymbol{v}; \boldsymbol{\mu}] = \sum_{q=1}^{Q_{\mathtt{f}}} \theta_{\mathtt{f}}^q(\boldsymbol{\mu})\, f^q[\boldsymbol{v}], \tag{2.12}$$

$$\boldsymbol{s}_\infty[\boldsymbol{u}, \boldsymbol{\mu}_s] = \sum_{q=1}^{Q_\infty} \theta_\infty^q(\boldsymbol{\mu}_s)\, \boldsymbol{s}_\infty^q[\boldsymbol{u}]. \tag{2.13}$$

Thus we impose a separation of parameter-dependent scalar functions $\theta_{\mathtt{a}}^q$, $\theta_{\mathtt{f}}^q$, $\theta_\infty^q$ and parameter-independent forms $a^q$, $f^q$, $\boldsymbol{s}_\infty^q$. This assumption allows for an offline/online separation where we compute the reduced basis and assemble the parameter-independent $(N\times N)$-dimensional matrices $\mathbf{A}^q$ and the $N$-dimensional vectors $\mathbf{F}^q, \boldsymbol{S}_\infty^q$ during the offline phase.

During the online procedure, (2.9) then takes the following form: for any new parameter value $\boldsymbol{\mu} \in \boldsymbol{\mathcal{P}}$, assemble the $(N\times N)$-dimensional matrix and $N$-dimensional vectors

$$\boldsymbol{A}(\boldsymbol{\mu}) = \sum_{q=1}^{Q_{\mathtt{a}}} \theta_{\mathtt{a}}^q(\boldsymbol{\mu})\, \mathbf{A}^q,$$

$$\boldsymbol{F}(\boldsymbol{\mu}) = \sum_{q=1}^{Q_{\mathtt{f}}} \theta_{\mathtt{f}}^q(\boldsymbol{\mu})\, \mathbf{F}^q,$$

$$\boldsymbol{S}_\infty(\boldsymbol{\mu}_s) = \sum_{q=1}^{Q_\infty} \theta_\infty^q(\boldsymbol{\mu}_s)\, \boldsymbol{S}_\infty^q,$$

solve the $N$-dimensional linear system

$$\boldsymbol{A}(\boldsymbol{\mu})\, \boldsymbol{U}_N(\boldsymbol{\mu}) = \boldsymbol{F}(\boldsymbol{\mu}),$$

and compute the RCS-signature

$$\boldsymbol{s}_\infty[\boldsymbol{u}_N(\boldsymbol{\mu}), \boldsymbol{\mu}_s] = \boldsymbol{S}_\infty(\boldsymbol{\mu}_s)^T\, \boldsymbol{U}_N(\boldsymbol{\mu}),$$

$$\mathrm{rcs}[\boldsymbol{u}_N(\boldsymbol{\mu}), \boldsymbol{\mu}, \boldsymbol{\mu}_s] = 10 \log_{10}\left(4\pi \frac{|\boldsymbol{s}_\infty[\boldsymbol{u}_N(\boldsymbol{\mu}); \boldsymbol{\mu}_s]|^2}{|\boldsymbol{E}^{\mathrm{inc}}(\boldsymbol{\mu})|^2}\right).$$

Observe that the online procedure is independent of $\mathcal{N}$ and, thus, can be computed at limited computational cost.

Observe that the affine decomposition cannot be satisfied in an exact manner for the sesquilinear and linear forms $a[\cdot, \cdot; \boldsymbol{\mu}]$, $f[\cdot; \boldsymbol{\mu}]$, and $\boldsymbol{s}_\infty[\cdot; \boldsymbol{\mu}_s]$. This can be overcome by using the empirical interpolation method (EIM) to satisfy the condition in an approximative manner to any desired tolerance. For more information on how to apply the EIM in this context, we refer the reader to [5, section 5] for a detailed discussion.

**3. Certified online error estimation.** Having discussed the core elements of the algorithm above, let us in the following develop the a posteriori error estimator and discuss its implementation in an online manner that allows for a fast and accurate evaluation of the estimator to certify the accuracy of the output of interest.

**3.1. Certified a posteriori estimation.** The goal of this section is to construct the a posteriori error indicator $\eta(\boldsymbol{\mu})$, required during the greedy construction to assemble the reduced basis and during the online procedure to certify a certain error tolerance of the error

$$\|\boldsymbol{u}_h(\boldsymbol{\mu}) - \boldsymbol{u}_N(\boldsymbol{\mu})\|_{\boldsymbol{X}_h},$$

where $\|\cdot\|_{\boldsymbol{X}_h}$ is a suitable norm for $\boldsymbol{X}_h$ with scalar product $(\cdot, \cdot)_{\boldsymbol{X}_h}$.

For the sake of completeness we repeat the common theory (Propositions 3.1 and 3.2) before we elaborate on problem specific versions for the output functional. Let $\boldsymbol{e}(\boldsymbol{\mu}) = \boldsymbol{u}_h(\boldsymbol{\mu}) - \boldsymbol{u}_N(\boldsymbol{\mu}) \in \boldsymbol{X}_h$ be the error function satisfying

$$a[\boldsymbol{e}(\boldsymbol{\mu}), \boldsymbol{v}_h; \boldsymbol{\mu}] = r[\boldsymbol{v}_h; \boldsymbol{\mu}] \qquad \forall \boldsymbol{v}_h \in \boldsymbol{X}_h,$$

where $r[\cdot; \boldsymbol{\mu}] \in \boldsymbol{X}_h'$ is the residual

$$r[\boldsymbol{v}_h; \boldsymbol{\mu}] = \boldsymbol{f}[\boldsymbol{v}_h; \boldsymbol{\mu}] - a[\boldsymbol{u}_N(\boldsymbol{\mu}), \boldsymbol{v}_h; \boldsymbol{\mu}] \qquad \forall \boldsymbol{v}_h \in \boldsymbol{X}_h.$$

Referring to its Riesz representation $\hat{\boldsymbol{e}}(\boldsymbol{\mu}) \in \boldsymbol{X}_h$ yields

$$(\hat{\boldsymbol{e}}(\boldsymbol{\mu}), \boldsymbol{v}_h)_{\boldsymbol{X}_h} = r[\boldsymbol{v}_h; \boldsymbol{\mu}] \qquad \forall \boldsymbol{v}_h \in \boldsymbol{X}_h,$$

and thus

$$a[\boldsymbol{e}(\boldsymbol{\mu}), \boldsymbol{v}_h; \boldsymbol{\mu}] = (\hat{\boldsymbol{e}}(\boldsymbol{\mu}), \boldsymbol{v}_h)_{\boldsymbol{X}_h}. \tag{3.1}$$

In addition, by definition of the operator norm we have

$$\|r[\cdot; \boldsymbol{\mu}]\|_{\boldsymbol{X}_h'} = \sup_{\boldsymbol{v}_h \in \boldsymbol{X}_h} \frac{r[\boldsymbol{v}_h; \boldsymbol{\mu}]}{\|\boldsymbol{v}_h\|_{\boldsymbol{X}_h}} = \|\hat{\boldsymbol{e}}(\boldsymbol{\mu})\|_{\boldsymbol{X}_h}.$$

Under the assumption that (2.10) is uniquely solvable, the following holds: for each $\boldsymbol{\mu} \in \boldsymbol{\mathcal{P}}$, there exists a $\beta_h(\boldsymbol{\mu}) > 0$ such that

$$\beta_h(\boldsymbol{\mu}) \|\boldsymbol{v}_h\|_{\boldsymbol{X}_h} \leq \sup_{\boldsymbol{w}_h \in \boldsymbol{X}_h} \frac{a[\boldsymbol{v}_h, \boldsymbol{w}_h; \boldsymbol{\mu}]}{\|\boldsymbol{w}_h\|_{\boldsymbol{X}_h}} \qquad \forall \boldsymbol{v}_h \in \boldsymbol{X}_h. \tag{3.2}$$

Now, assuming that we, independently of $\mathcal{N}$, can compute a lower bound $0 < \beta_{\mathtt{LB}}(\boldsymbol{\mu}) \leq \beta_h(\boldsymbol{\mu})$ for any $\boldsymbol{\mu} \in \boldsymbol{\mathcal{P}}$, we define the a posteriori estimate as

$$\eta_N(\boldsymbol{\mu}) = \frac{\|\hat{\boldsymbol{e}}(\boldsymbol{\mu})\|_{\boldsymbol{X}_h}}{\beta_{\mathtt{LB}}(\boldsymbol{\mu})}. \tag{3.3}$$

PROPOSITION 3.1 (see [10]). *The a posteriori estimator defined in* (3.3) *is reliable, i.e.,*

$$\|\boldsymbol{u}_h(\boldsymbol{\mu}) - \boldsymbol{u}_N(\boldsymbol{\mu})\|_{\boldsymbol{X}_h} \leq \eta_N(\boldsymbol{\mu}).$$

*Proof.* Indeed, combining the inf-sup condition (3.2) with (3.1) yields

$$\beta_h(\boldsymbol{\mu}) \, \|\boldsymbol{e}(\boldsymbol{\mu})\|_{\boldsymbol{X}_h} \leq \sup_{\boldsymbol{w}_h \in \boldsymbol{X}_h} \frac{a[\boldsymbol{e}(\boldsymbol{\mu}), \boldsymbol{w}_h; \boldsymbol{\mu}]}{\|\boldsymbol{w}_h\|_{\boldsymbol{X}_h}} = \sup_{\boldsymbol{w}_h \in \boldsymbol{X}_h} \frac{(\hat{\boldsymbol{e}}(\boldsymbol{\mu}), \boldsymbol{w}_h)_{\boldsymbol{X}_h}}{\|\boldsymbol{w}_h\|_{\boldsymbol{X}_h}} \leq \|\hat{\boldsymbol{e}}(\boldsymbol{\mu})\|_{\boldsymbol{X}_h},$$

and thus

$$\|\boldsymbol{e}(\boldsymbol{\mu})\|_{\boldsymbol{X}_h} \leq \tfrac{1}{\beta_h(\boldsymbol{\mu})} \|\hat{\boldsymbol{e}}(\boldsymbol{\mu})\|_{\boldsymbol{X}_h} \leq \tfrac{1}{\beta_{\mathtt{LB}}(\boldsymbol{\mu})} \|\hat{\boldsymbol{e}}(\boldsymbol{\mu})\|_{\boldsymbol{X}_h} = \eta_N(\boldsymbol{\mu}). \qquad \square$$

Under the condition that for the given norm $\|\cdot\|_{\boldsymbol{X}_h}$, the form $a[\cdot, \cdot; \boldsymbol{\mu}]$ is also continuous, that is, for each $\boldsymbol{\mu} \in \boldsymbol{\mathcal{P}}$, there exists a constant $\gamma_h(\boldsymbol{\mu}) > 0$ such that

$$a[\boldsymbol{v}_h, \boldsymbol{w}_h; \boldsymbol{\mu}] \leq \gamma_h(\boldsymbol{\mu}) \, \|\boldsymbol{v}_h\|_{\boldsymbol{X}_h} \|\boldsymbol{w}_h\|_{\boldsymbol{X}_h} \qquad \forall \boldsymbol{v}_h, \boldsymbol{w}_h \in \boldsymbol{X}_h,$$

one can prove the following efficiency result.

PROPOSITION 3.2 (see [10]). *The a posteriori estimator defined in* (3.3) *is efficient, i.e.,*

$$\eta_N(\boldsymbol{\mu}) \leq \tfrac{\gamma_h(\boldsymbol{\mu})}{\beta_{\mathtt{LB}}(\boldsymbol{\mu})} \|\boldsymbol{e}(\boldsymbol{\mu})\|_{\boldsymbol{X}_h}.$$

*Proof.* Given that

$$\|\hat{\boldsymbol{e}}(\boldsymbol{\mu})\|_{\boldsymbol{X}_h}^2 = a[\boldsymbol{e}(\boldsymbol{\mu}), \hat{\boldsymbol{e}}(\boldsymbol{\mu}); \boldsymbol{\mu}] \leq \gamma_h(\boldsymbol{\mu}) \, \|\boldsymbol{e}(\boldsymbol{\mu})\|_{\boldsymbol{X}_h} \, \|\hat{\boldsymbol{e}}(\boldsymbol{\mu})\|_{\boldsymbol{X}_h},$$

we conclude that

$$\eta_N(\boldsymbol{\mu}) = \tfrac{1}{\beta_{\text{LB}}(\boldsymbol{\mu})}\|\hat{\boldsymbol{e}}(\boldsymbol{\mu})\|_{\boldsymbol{X}_h} \le \tfrac{\gamma_h(\boldsymbol{\mu})}{\beta_{\text{LB}}(\boldsymbol{\mu})}\|\boldsymbol{e}(\boldsymbol{\mu})\|_{\boldsymbol{X}_h}. \qquad \square$$

Now, we turn our attention to the particular case where the discrete space $\boldsymbol{X}_h$ is defined by (2.6). In this case, the intrinsic solution space $\boldsymbol{X}$ is the space $\boldsymbol{H}^{-\frac{1}{2}}(\text{div}_\Gamma, \Gamma)$ (see [2, 7]), which induces a natural norm for the discrete space $\boldsymbol{X}_h$. Here the operator $\text{div}_\Gamma$ denotes the surface divergence. As we discussed previously, the computation of the $\boldsymbol{H}^{-\frac{1}{2}}(\text{div}_\Gamma, \Gamma)$-norm involves the single layer boundary potential integral operator for the Laplacian, which is relatively expensive in practice. Observe that the norm is used to compute the error between the truth solution and the reduced basis approximation, both being discrete and belonging to $\boldsymbol{X}_h$. The discrete approximation space $\boldsymbol{X}_h$ is a subspace of $\boldsymbol{H}(\text{div}_\Gamma, \Gamma)$, and it is therefore natural to alternatively consider the norm $\|\cdot\|_{\boldsymbol{X}_h}$ defined by

$$\|\boldsymbol{v}_h\|^2_{\boldsymbol{X}_h} = \|\boldsymbol{v}_h\|^2_{L^2(\Gamma)} + \|\text{div}_\Gamma \boldsymbol{v}_h\|^2_{L^2(\Gamma)} \qquad \forall \boldsymbol{v}_h \in \boldsymbol{X}_h.$$

In what follows, we shall use this norm to measure the error. It shall be noticed that all that follows also holds if one decides to use a norm of $\boldsymbol{H}^{-\frac{1}{2}}(\text{div}_\Gamma, \Gamma)$.

PROPOSITION 3.3. *The error in the output functional $\boldsymbol{s}_\infty$ is certified by the following computable error bound:*

$$|\boldsymbol{s}_\infty[\boldsymbol{u}_h(\boldsymbol{\mu}); \boldsymbol{\mu}_s] - \boldsymbol{s}_\infty[\boldsymbol{u}_N(\boldsymbol{\mu}); \boldsymbol{\mu}_s]| < \tfrac{kZ|\Gamma|^{\frac{1}{2}}}{4\pi}\eta_N(\boldsymbol{\mu}).$$

*Proof.* By linearity of $\boldsymbol{s}_\infty$ and Proposition 3.1, observe that the following bound holds:

$$\begin{aligned}
|\boldsymbol{s}_\infty[\boldsymbol{u}_h(\boldsymbol{\mu}); \boldsymbol{\mu}_s] - \boldsymbol{s}_\infty[\boldsymbol{u}_N(\boldsymbol{\mu}); \boldsymbol{\mu}_s]| &= |\boldsymbol{s}_\infty[\boldsymbol{u}_h(\boldsymbol{\mu}) - \boldsymbol{u}_N(\boldsymbol{\mu}); \boldsymbol{\mu}_s]| \\
&\le \|s_\infty[\cdot; k, \hat{\boldsymbol{d}}_0]\|_{\boldsymbol{X}_h'} \, \|\boldsymbol{u}_h(\boldsymbol{\mu}) - \boldsymbol{u}_N(\boldsymbol{\mu})\|_{\boldsymbol{X}_h} \\
&\le \|s_\infty[\cdot; k, \hat{\boldsymbol{d}}_0]\|_{\boldsymbol{X}_h'} \, \eta_N(\boldsymbol{\mu}),
\end{aligned}$$

where the operator norm can be estimated by

$$\begin{aligned}
\|s_\infty[\cdot; k, \hat{\boldsymbol{d}}_0]\|_{\boldsymbol{X}_h'} &= \sup_{\boldsymbol{w}_h \in \boldsymbol{X}_h} \frac{|s_\infty[\boldsymbol{w}_h; k, \hat{\boldsymbol{d}}_0]|}{\|\boldsymbol{w}_h\|_{\boldsymbol{X}_h}} \\
&= \frac{kZ}{4\pi} \sup_{\boldsymbol{w}_h \in \boldsymbol{X}_h} \frac{|\int_\Gamma \hat{\boldsymbol{d}}_0 \times (\boldsymbol{w}_h(\boldsymbol{x}; \boldsymbol{\mu}) \times \hat{\boldsymbol{d}}_0) e^{ik\boldsymbol{x}\cdot\hat{\boldsymbol{d}}_0} \, d\boldsymbol{x}|}{\|\boldsymbol{w}_h\|_{\boldsymbol{X}_h}} \\
&\le \frac{kZ}{4\pi} \sup_{\boldsymbol{w}_h \in \boldsymbol{X}_h} \frac{|\int_\Gamma \boldsymbol{w}_h(\boldsymbol{x}; \boldsymbol{\mu}) e^{ik\boldsymbol{x}\cdot\hat{\boldsymbol{d}}_0} \, d\boldsymbol{x}|}{\|\boldsymbol{w}_h\|_{\boldsymbol{X}_h}} \le \frac{kZ}{4\pi} \sup_{\boldsymbol{w}_h \in \boldsymbol{X}_h} \frac{\|\boldsymbol{w}_h\|_{L^2(\Gamma)} \|1\|_{L^2(\Gamma)}}{\|\boldsymbol{w}_h\|_{\boldsymbol{X}_h}} \\
&= \frac{kZ|\Gamma|^{\frac{1}{2}}}{4\pi} \sup_{\boldsymbol{w}_h \in \boldsymbol{X}_h} \frac{\|\boldsymbol{w}_h\|_{L^2(\Gamma)}}{\|\boldsymbol{w}_h\|_{\boldsymbol{X}_h}} \le \frac{kZ|\Gamma|^{\frac{1}{2}}}{4\pi}. \qquad \square
\end{aligned}$$

COROLLARY 3.4. *If $\boldsymbol{s}_\infty[\boldsymbol{u}_N(\boldsymbol{\mu}); \boldsymbol{\mu}_s]$ and the error certification $\varepsilon_s = \frac{kZ|\Gamma|^{1/2}}{4\pi}\eta_N(\boldsymbol{\mu})$ are given, the truth functional $\boldsymbol{s}_\infty[\boldsymbol{u}_h(\boldsymbol{\mu}); \boldsymbol{\mu}_s]$ lies within the error bars*

$$\boldsymbol{s}_\infty[\boldsymbol{u}_N(\boldsymbol{\mu}); \boldsymbol{\mu}_s] - \varepsilon_s \le \boldsymbol{s}_\infty[\boldsymbol{u}_h(\boldsymbol{\mu}); \boldsymbol{\mu}_s] \le \boldsymbol{s}_\infty[\boldsymbol{u}_N(\boldsymbol{\mu}); \boldsymbol{\mu}_s] + \varepsilon_s.$$

PROPOSITION 3.5. *The error in the RCS is certified by the following computable error bound:*

$$\begin{aligned}|\mathrm{rcs}[\boldsymbol{u}_h(\boldsymbol{\mu});\boldsymbol{\mu},\boldsymbol{\mu}_s] - \mathrm{rcs}[\boldsymbol{u}_N(\boldsymbol{\mu});\boldsymbol{\mu},\boldsymbol{\mu}_s]| \\ \leq 20\max\left(\log_{10}\left(\frac{|\boldsymbol{s}_\infty[\boldsymbol{u}_N(\boldsymbol{\mu});\boldsymbol{\mu}_s]| + \varepsilon_s}{|\boldsymbol{s}_\infty[\boldsymbol{u}_N(\boldsymbol{\mu});\boldsymbol{\mu}_s]|}\right),\right. \\ \left.\log_{10}\left(\frac{|\boldsymbol{s}_\infty[\boldsymbol{u}_N(\boldsymbol{\mu});\boldsymbol{\mu}_s]|}{|\boldsymbol{s}_\infty[\boldsymbol{u}_N(\boldsymbol{\mu});\boldsymbol{\mu}_s]| - \varepsilon_s}\right)\right).\end{aligned}$$

*Proof.* Using properties of the logarithmic function, note that

$$\begin{aligned}&\mathrm{rcs}[\boldsymbol{u}_h(\boldsymbol{\mu});\boldsymbol{\mu},\boldsymbol{\mu}_s] - \mathrm{rcs}[\boldsymbol{u}_N(\boldsymbol{\mu});\boldsymbol{\mu},\boldsymbol{\mu}_s] \\ &\quad= 10\left(\log_{10}\left(4\pi\frac{|\boldsymbol{s}_\infty[\boldsymbol{u}_h(\boldsymbol{\mu});\boldsymbol{\mu}_s]|^2}{|\boldsymbol{E}^{\mathrm{inc}}(\boldsymbol{\mu})|^2}\right) - \log_{10}\left(4\pi\frac{|\boldsymbol{s}_\infty[\boldsymbol{u}_N(\boldsymbol{\mu});\boldsymbol{\mu}_s]|^2}{|\boldsymbol{E}^{\mathrm{inc}}(\boldsymbol{\mu})|^2}\right)\right) \\ &\quad= 20\left(\log_{10}\left(|\boldsymbol{s}_\infty[\boldsymbol{u}_h(\boldsymbol{\mu});\boldsymbol{\mu}_s]|\right) - \log_{10}\left(|\boldsymbol{s}_\infty[\boldsymbol{u}_N(\boldsymbol{\mu});\boldsymbol{\mu}_s]|\right)\right) \\ &\quad= 20\log_{10}\left(\frac{|\boldsymbol{s}_\infty[\boldsymbol{u}_h(\boldsymbol{\mu});\boldsymbol{\mu}_s]|}{|\boldsymbol{s}_\infty[\boldsymbol{u}_N(\boldsymbol{\mu});\boldsymbol{\mu}_s]|}\right).\end{aligned}$$

From the bound

$$|\boldsymbol{s}_\infty[\boldsymbol{u}_h(\boldsymbol{\mu});\boldsymbol{\mu}_s] - \boldsymbol{s}_\infty[\boldsymbol{u}_N(\boldsymbol{\mu});\boldsymbol{\mu}_s]| < \varepsilon_s$$

and using the inverse triangle inequality, we recover the error bars

$$\frac{|\boldsymbol{s}_\infty[\boldsymbol{u}_N(\boldsymbol{\mu});\boldsymbol{\mu}_s]| - \varepsilon_s}{|\boldsymbol{s}_\infty[\boldsymbol{u}_N(\boldsymbol{\mu});\boldsymbol{\mu}_s]|} < \frac{|\boldsymbol{s}_\infty[\boldsymbol{u}_h(\boldsymbol{\mu});\boldsymbol{\mu}_s]|}{|\boldsymbol{s}_\infty[\boldsymbol{u}_N(\boldsymbol{\mu});\boldsymbol{\mu}_s]|} < \frac{|\boldsymbol{s}_\infty[\boldsymbol{u}_N(\boldsymbol{\mu});\boldsymbol{\mu}_s]| + \varepsilon_s}{|\boldsymbol{s}_\infty[\boldsymbol{u}_N(\boldsymbol{\mu});\boldsymbol{\mu}_s]|}.$$

Thus, we have the estimate

$$\begin{aligned}&|\mathrm{rcs}[\boldsymbol{u}_h(\boldsymbol{\mu});\boldsymbol{\mu},\boldsymbol{\mu}_s] - \mathrm{rcs}[\boldsymbol{u}_N(\boldsymbol{\mu});\boldsymbol{\mu},\boldsymbol{\mu}_s]| \\ &= 20\max\left(\log_{10}\left(\frac{|\boldsymbol{s}_\infty[\boldsymbol{u}_h(\boldsymbol{\mu});\boldsymbol{\mu}_s]|}{|\boldsymbol{s}_\infty[\boldsymbol{u}_N(\boldsymbol{\mu});\boldsymbol{\mu}_s]|}\right), \log_{10}\left(\frac{|\boldsymbol{s}_\infty[\boldsymbol{u}_N(\boldsymbol{\mu});\boldsymbol{\mu}_s]|}{|\boldsymbol{s}_\infty[\boldsymbol{u}_h(\boldsymbol{\mu});\boldsymbol{\mu}_s]|}\right)\right) \\ &\leq 20\max\left(\log_{10}\left(\frac{|\boldsymbol{s}_\infty[\boldsymbol{u}_N(\boldsymbol{\mu});\boldsymbol{\mu}_s]| + \varepsilon_s}{|\boldsymbol{s}_\infty[\boldsymbol{u}_N(\boldsymbol{\mu});\boldsymbol{\mu}_s]|}\right), \log_{10}\left(\frac{|\boldsymbol{s}_\infty[\boldsymbol{u}_N(\boldsymbol{\mu});\boldsymbol{\mu}_s]|}{|\boldsymbol{s}_\infty[\boldsymbol{u}_N(\boldsymbol{\mu});\boldsymbol{\mu}_s]| - \varepsilon_s}\right)\right).\end{aligned}$$

∎

**3.2. Efficient implementation of the error estimator.** Under the assumption that the lower bound of the inf-sup constant is computable for any parameter value, independently of the dimension of the boundary element space $\mathcal{N}$, we discuss in this section how the error estimation $\eta(\boldsymbol{\mu})$ can likewise be evaluated online, independently of $\mathcal{N}$. The computation of the inf-sup constant is addressed in section 3.3.

Given the affine decompositions (2.11), (2.12), we write

$$\begin{aligned}(\hat{\boldsymbol{e}}(\boldsymbol{\mu}),\boldsymbol{v}_h)_{\boldsymbol{X}_h} &= r[\boldsymbol{v}_h;\boldsymbol{\mu}] = f[\boldsymbol{v}_h;\boldsymbol{\mu}] - a[\boldsymbol{u}_N(\boldsymbol{\mu}),\boldsymbol{v}_h;\boldsymbol{\mu}] \\ &= \sum_{q=1}^{Q_{\mathtt{f}}} \theta_{\mathtt{f}}^q(\boldsymbol{\mu})\, f^q[\boldsymbol{v}_h] - \sum_{q=1}^{Q_{\mathtt{a}}} \theta_{\mathtt{a}}^q(\boldsymbol{\mu})\, a^q[\boldsymbol{u}_N,\boldsymbol{v}_h] \\ &= \sum_{q=1}^{Q_{\mathtt{f}}} \theta_{\mathtt{f}}^q(\boldsymbol{\mu})\, f^q[\boldsymbol{v}_h] - \sum_{n=1}^{N}\sum_{q=1}^{Q_{\mathtt{a}}} u_n \theta_{\mathtt{a}}^q(\boldsymbol{\mu})\, a^q[\boldsymbol{\xi}_n,\boldsymbol{v}_h],\end{aligned}$$

where $\{\xi_n\}_{n=1}^N$ are basis functions of the reduced basis space $\boldsymbol{X}_N$ and $\{u_n\}_{n=1}^N \subset \mathbb{C}$ are the degrees of freedom with respect to $\{\xi_n\}_{n=1}^N$. Thus, we have

$$\hat{\boldsymbol{e}}(\boldsymbol{\mu}) = \sum_{q=1}^{Q_{\mathtt{f}}} \theta_{\mathtt{f}}^q(\boldsymbol{\mu})\, \mathtt{f}^q - \sum_{n=1}^{N} \sum_{q=1}^{Q_{\mathtt{a}}} u_n \theta_{\mathtt{a}}^q(\boldsymbol{\mu})\, \mathtt{a}^{q,n},$$

with $\mathtt{f}^q, \mathtt{a}^{q,n} \in \boldsymbol{X}_h$ such that

$$(\mathtt{f}^q, \boldsymbol{v}_h)_{\boldsymbol{X}_h} = f^q[\boldsymbol{v}_h],$$
$$(\mathtt{a}^{q,n}, \boldsymbol{v}_h)_{\boldsymbol{X}_h} = a^q[\boldsymbol{\xi}_n, \boldsymbol{v}_h]$$

for all $\boldsymbol{v}_h \in \boldsymbol{X}_h$ using the Riesz representation theorem. In practice, this corresponds to solving a linear system using the matrix associated with the scalar product $(\cdot,\cdot)_{\boldsymbol{X}_h}$. We finally write

$$\begin{aligned}\|\hat{\boldsymbol{e}}(\boldsymbol{\mu})\|_{\boldsymbol{X}_h}^2 \;=\; & \sum_{q,m=1}^{Q_{\mathtt{f}}} \overline{\theta_{\mathtt{f}}^q(\boldsymbol{\mu})}\theta_{\mathtt{f}}^m(\boldsymbol{\mu})\, (\mathtt{f}^q, \mathtt{f}^m)_{\boldsymbol{X}_h} \\ & - 2\Re\left[\sum_{n=1}^{N}\sum_{m=1}^{Q_{\mathtt{f}}}\sum_{q=1}^{Q_{\mathtt{a}}} u_n\, \overline{\theta_{\mathtt{f}}^m(\boldsymbol{\mu})}\theta_{\mathtt{a}}^q(\boldsymbol{\mu})\, (\mathtt{f}^m, \mathtt{a}^{q,n})_{\boldsymbol{X}_h}\right] \\ & + \sum_{n,k=1}^{N}\sum_{q,m=1}^{Q_{\mathtt{a}}} u_n u_k\, \overline{\theta_{\mathtt{a}}^q(\boldsymbol{\mu})}\theta_{\mathtt{a}}^m(\boldsymbol{\mu})\, (\mathtt{a}^{q,n}, \mathtt{a}^{m,k})_{\boldsymbol{X}_h}.\end{aligned}$$

Now, one can observe that the quantities

$$\mathtt{R}^1_{q,m} = (\mathtt{f}^q, \mathtt{f}^m)_{\boldsymbol{X}_h}, \qquad \mathtt{R}^2_{m,q,n} = (\mathtt{f}^m, \mathtt{a}^{q,n})_{\boldsymbol{X}_h}, \qquad \mathtt{R}^3_{q,n,m,k} = (\mathtt{a}^{q,n}, \mathtt{a}^{m,k})_{\boldsymbol{X}_h}$$

can be precomputed, i.e., they are parameter independent during the offline process, once the reduced basis is assembled. Therefore the a posteriori estimate can be computed independently of $\mathcal{N}$ by

$$\begin{aligned}\eta(\boldsymbol{\mu}) = \frac{1}{\beta_{\mathtt{LB}}(\boldsymbol{\mu})}\Bigg(\sum_{q,m=1}^{Q_{\mathtt{f}}} \overline{\theta_{\mathtt{f}}^q(\boldsymbol{\mu})}\theta_{\mathtt{f}}^m(\boldsymbol{\mu})\, \mathtt{R}^1_{q,m} - 2\Re\left[\sum_{n=1}^{N}\sum_{m=1}^{Q_{\mathtt{f}}}\sum_{q=1}^{Q_{\mathtt{a}}} u_n\, \overline{\theta_{\mathtt{f}}^m(\boldsymbol{\mu})}\theta_{\mathtt{a}}^q(\boldsymbol{\mu})\, \mathtt{R}^2_{m,q,n}\right] \\ + \sum_{n,k=1}^{N}\sum_{q,m=1}^{Q_{\mathtt{a}}} u_n u_k\, \overline{\theta_{\mathtt{a}}^q(\boldsymbol{\mu})}\theta_{\mathtt{a}}^m(\boldsymbol{\mu})\, \mathtt{R}^3_{q,n,m,k}\Bigg)^{\frac{1}{2}}. \qquad (3.4)\end{aligned}$$

**3.3. Implementation of the successive constraint method for complex matrices.** The successive constraint method (SCM) is an offline-online procedure where the online part consists of providing, for each new parameter value $\boldsymbol{\mu} \in \boldsymbol{\mathcal{P}}$, a lower bound $\beta_{\mathtt{LB}}$ (and upper bound $\beta_{\mathtt{UB}}$) of the inf-sup constant defined by (3.2), i.e., $0 < \beta_{\mathtt{LB}}(\boldsymbol{\mu}) \le \beta_h(\boldsymbol{\mu}) \le \beta_{\mathtt{UB}}(\boldsymbol{\mu})$. The SCM is discussed in [8, 3, 4], but for the sake of completeness we present the method in full detail here. Different from the presentation in [3], where the real and imaginary parts of a complex matrix are decoupled in the SCM, we enhance the algorithm by fully utilizing properties of the Hermitian matrices.

The underlying idea of the SCM is that computing the inf-sup constant can be viewed as an optimization problem. We first note that the inf-sup constant introduced

in (3.2) can be properly written as

$$\beta_h(\boldsymbol{\mu}) = \inf_{\boldsymbol{v}_h \in \boldsymbol{X}_h} \sup_{\boldsymbol{w}_h \in \boldsymbol{X}_h} \frac{a[\boldsymbol{v}_h, \boldsymbol{w}_h; \boldsymbol{\mu}]}{\|\boldsymbol{v}_h\|_{\boldsymbol{X}_h} \|\boldsymbol{w}_h\|_{\boldsymbol{X}_h}}.$$

Introducing the operator $\mathtt{A}(\boldsymbol{\mu}) : \boldsymbol{X}_h \mapsto \boldsymbol{X}_h$ associated with the sesquilinear form $a[\cdot, \cdot; \boldsymbol{\mu}] : \boldsymbol{X}_h \times \boldsymbol{X}_h \mapsto \mathbb{C}$ such that $(\mathtt{A}(\boldsymbol{\mu})\boldsymbol{v}_h, \boldsymbol{w}_h)_{\boldsymbol{X}_h} = a[\boldsymbol{v}_h, \boldsymbol{w}_h; \boldsymbol{\mu}]$ for all $\boldsymbol{v}_h, \boldsymbol{w}_h \in \boldsymbol{X}_h$, we notice that

$$\beta_h(\boldsymbol{\mu}) = \inf_{\boldsymbol{v}_h \in \boldsymbol{X}_h} \frac{\|\mathtt{A}(\boldsymbol{\mu})\boldsymbol{v}_h\|_{\boldsymbol{X}_h}}{\|\boldsymbol{v}_h\|_{\boldsymbol{X}_h}}.$$

Squaring the previous expression results in

$$(\beta_h(\boldsymbol{\mu}))^2 = \inf_{\boldsymbol{v}_h \in \boldsymbol{X}_h} \frac{(\mathtt{A}(\boldsymbol{\mu})\boldsymbol{v}_h, \mathtt{A}(\boldsymbol{\mu})\boldsymbol{v}_h)_{\boldsymbol{X}_h}}{\|\boldsymbol{v}_h\|^2_{\boldsymbol{X}_h}}.$$

We are therefore interested in computing the lowest generalized eigenvalue of the parameter-dependent matrix $\mathtt{A}^*\mathtt{A}(\boldsymbol{\mu})$.

**3.3.1. Offline procedure of SCM.** Assume for now that the matrix $\mathtt{A}^*\mathtt{A}$ is a linear combination of semipositive Hermitian matrices, i.e.,

$$\mathtt{A}^*\mathtt{A}(\boldsymbol{\mu}) = \sum_{\hat{q}=1}^{\hat{Q}} z_{\hat{q}}(\boldsymbol{\mu}) \mathtt{Z}_{\hat{q}}, \tag{3.5}$$

such that all $z_{\hat{q}}$ are real and $\mathtt{Z}_{\hat{q}}$ is Hermitian, and thus has only real eigenvalues. This is a key feature of the SCM, and a way to achieve this is discussed in section 3.3.3. We can then continue in a standard fashion as described in [3] by noting that

$$\alpha_h(\boldsymbol{\mu}) = \inf_{\boldsymbol{v}_h \in \boldsymbol{X}_h} \sum_{\hat{q}=1}^{\hat{Q}} z_{\hat{q}}(\boldsymbol{\mu}) \frac{(\boldsymbol{v}_h, \mathtt{Z}_{\hat{q}}\boldsymbol{v}_h)_{\boldsymbol{X}_h}}{\|\boldsymbol{v}_h\|^2_{\boldsymbol{X}_h}} \tag{3.6}$$

for $\alpha_h(\boldsymbol{\mu}) = (\beta_h(\boldsymbol{\mu}))^2$.

The underlying idea of the SCM is to interpret the right-hand side of (3.6) as a minimization problem of the functional

$$\mathtt{I} : \boldsymbol{\mathcal{P}} \times \mathbb{R}^{\hat{Q}} \longrightarrow \mathbb{R},$$
$$(\boldsymbol{\mu}, \boldsymbol{y}) \longmapsto \mathtt{I}(\boldsymbol{\mu}, \boldsymbol{y}) = \sum_{\hat{q}=1}^{\hat{Q}} z_{\hat{q}}(\boldsymbol{\mu})\, y_{\hat{q}}$$

over the set of admissible solutions

$$\boldsymbol{\mathcal{Y}} = \left\{ \boldsymbol{y} = (y_1, \ldots, y_{\hat{Q}}) \in \mathbb{R}^{\hat{Q}} \;\middle|\; \exists\, \boldsymbol{v}_h \in \boldsymbol{X}_h \text{ such that } y_{\hat{q}} = \frac{(\boldsymbol{v}_h, \mathtt{Z}_{\hat{q}}\boldsymbol{v}_h)_{\boldsymbol{X}_h}}{\|\boldsymbol{v}_h\|^2_{\boldsymbol{X}_h}}, 1 \le \hat{q} \le \hat{Q} \right\}.$$

Then,

$$\alpha_h(\boldsymbol{\mu}) = \min_{\boldsymbol{y} \in \boldsymbol{\mathcal{Y}}} \mathtt{I}(\boldsymbol{\mu}, \boldsymbol{y})$$

and a lower and an upper bound can be found by enlarging (resp., restricting) the admissible set of solution vectors $\boldsymbol{y}$ by introducing $\boldsymbol{\mathcal{Y}}_{\mathtt{UB}} \subset \boldsymbol{\mathcal{Y}} \subset \boldsymbol{\mathcal{Y}}_{\mathtt{LB}}$ and then defining

$$\alpha_{\mathtt{LB}}(\boldsymbol{\mu}) = \min_{\boldsymbol{y}\in\boldsymbol{\mathcal{Y}}_{\mathtt{LB}}} \mathtt{I}(\boldsymbol{\mu},\boldsymbol{y}) \qquad \text{and} \qquad \alpha_{\mathtt{UB}}(\boldsymbol{\mu}) = \min_{\boldsymbol{y}\in\boldsymbol{\mathcal{Y}}_{\mathtt{UB}}} \mathtt{I}(\boldsymbol{\mu},\boldsymbol{y}).$$

The remaining question consists of how to design the spaces $\boldsymbol{\mathcal{Y}}_{\mathtt{UB}}$ and $\boldsymbol{\mathcal{Y}}_{\mathtt{LB}}$ in an easy way such that any target accuracy can be achieved for the quantity

$$1 - \frac{\alpha_{\mathtt{LB}}(\boldsymbol{\mu})}{\alpha_{\mathtt{UB}}(\boldsymbol{\mu})}. \tag{3.7}$$

As for the RBM, the SCM is an offline-online procedure where during the compute intensive offline stage generalized eigenvalue problems of size $\mathcal{N}$ need to be solved, where the online stage is $\mathcal{N}$-independent and thus can be used in combination with the online stage of the RBM, as explained in section 3.2.

Denote by $\boldsymbol{\mathcal{P}_a}$ the restriction of $\boldsymbol{\mathcal{P}}$ to the set of actively varying parameters of the form $a[\cdot,\cdot;\cdot]$. In our case the only active parameter for the sesquilinear form is the wave-number $k$. Then, the $n$th iteration of the offline procedure takes the following form assuming the following:

1. We know $\alpha_h(\boldsymbol{\mu}_j)$, $1 \le j \le n$, for some parameter values $\mathbb{C}_n = \{\boldsymbol{\mu}_1,\dots,\boldsymbol{\mu}_n\} \subset \boldsymbol{\mathcal{P}_a}$.
2. Let $\Xi \subset \boldsymbol{\mathcal{P}_a}$ be a fine and finite point-set discretization of $\boldsymbol{\mathcal{P}_a}$. For each $\boldsymbol{\mu} \in \Xi$, we know some lower bound $\alpha_{\mathtt{LB}}^{n-1}(\boldsymbol{\mu})$ of $\alpha_h(\boldsymbol{\mu})$ from the previous iteration. For $n = 1$, set $\alpha_{\mathtt{LB}}^{0}(\boldsymbol{\mu}) = 0$.

Thus $\alpha_h(\boldsymbol{\mu}_j)$ corresponds to the smallest eigenvalue of the generalized eigenvalue problem

$$\big(\boldsymbol{v}_h, \mathtt{A}^*\mathtt{A}(\boldsymbol{\mu}_j)\boldsymbol{w}_h^j\big)_{\boldsymbol{X}_h} = \alpha_h(\boldsymbol{\mu}_j)\big(\boldsymbol{v}_h, \boldsymbol{w}_h^j\big)_{\boldsymbol{X}_h} \qquad \forall \boldsymbol{v}_h \in \boldsymbol{X}_h. \tag{3.8}$$

The collection of smallest eigenvalues provides a set of eigenfunctions $\{\boldsymbol{w}_h^j\}_{j=1}^n$ and corresponding vectors $\{\boldsymbol{y}^j\}_{j=1}^n$ such that

$$(\boldsymbol{y}^j)_{\hat{q}} = \frac{(\boldsymbol{w}_h^j, \mathtt{Z}_{\hat{q}}\boldsymbol{w}_h^j)_{\boldsymbol{X}_h}}{\|\boldsymbol{w}_h^j\|_{\boldsymbol{X}_h}^2}, \qquad 1 \le \hat{q} \le \hat{Q},\ 1 \le j \le n.$$

Then, we set

$$\boldsymbol{\mathcal{Y}}_{\mathtt{UB}}^k(\mathbb{C}_n) = \left\{\boldsymbol{y}^j \,\middle|\, 1 \le j \le n\right\},$$

which is clearly a subset of $\boldsymbol{\mathcal{Y}}$. This means that for $\boldsymbol{\mathcal{Y}}_{\mathtt{UB}}$ we use a finite set of precomputed vectors $\boldsymbol{y}^j$. Also, computing $\alpha_{\mathtt{UB}}^n(\boldsymbol{\mu}) = \min_{\boldsymbol{y}\in\boldsymbol{\mathcal{Y}}_{\mathtt{UB}}^n} \mathtt{I}(\boldsymbol{\mu},\boldsymbol{y})$ consists only of forming the functional $\mathtt{I}$ for a finite number of $\boldsymbol{y}^j$, which is independent of $\mathcal{N}$.

On the other hand, for $\boldsymbol{\mathcal{Y}}_{\mathtt{LB}}$ we first define a rectangular box $\boldsymbol{\mathcal{B}} = \prod_{\hat{q}=1}^{\hat{Q}}[\sigma_{\hat{q}}^-, \sigma_{\hat{q}}^+] \subset \mathbb{R}^{\hat{Q}}$ that contains $\boldsymbol{\mathcal{Y}}$ by setting

$$\sigma_{\hat{q}}^- = \inf_{\boldsymbol{v}_h\in\boldsymbol{X}_h} \frac{(\boldsymbol{v}_h, \mathtt{Z}_{\hat{q}}\boldsymbol{v}_h)_{\boldsymbol{X}_h}}{\|\boldsymbol{v}_h\|_{\boldsymbol{X}_h}^2} \qquad \text{and} \qquad \sigma_{\hat{q}}^+ = \sup_{\boldsymbol{v}_h\in\boldsymbol{X}_h} \frac{(\boldsymbol{v}_h, \mathtt{Z}_{\hat{q}}\boldsymbol{v}_h)_{\boldsymbol{X}_h}}{\|\boldsymbol{v}_h\|_{\boldsymbol{X}_h}^2}.$$

This corresponds to the smallest and largest eigenvalues of a generalized eigenvalue problem for each $\hat{q}$ and can be computed once and for all in the beginning of the algorithm. However, in order to have a set $\boldsymbol{\mathcal{Y}}_{\mathtt{LB}}$ as small as possible and containing $\boldsymbol{\mathcal{Y}}$ we need to impose some additional restrictions. These constraints will depend on the value of the actual parameter $\boldsymbol{\mu}$, and we distinguish between two types:

1. constraints based on the exact eigenvalues for some close (in parameter space) parameters out of the set $\mathbb{C}_n$,
2. constraints based on the previous lower bounds $\alpha_{\mathtt{LB}}^{n-1}$ for some neighbor parameter values.

Observe that, in contrast to $\boldsymbol{\mathcal{Y}}_{\mathtt{UB}}$, the space $\boldsymbol{\mathcal{Y}}_{\mathtt{LB}}$ will change with variation of the parameter $\boldsymbol{\mu}$. We introduce the function that provides close parameter values

$$\mathbb{P}_M(\boldsymbol{\mu}; E) = \begin{cases} M \text{ closest points to } \boldsymbol{\mu} \text{ in } E & \text{if } \mathrm{card}(E) > M, \\ E & \text{if } \mathrm{card}(E) \leq M \end{cases}$$

for $E = \mathbb{C}_n$ and $E = \Xi$. For some $M_\alpha$ and $M_p$, we then define

$$\boldsymbol{\mathcal{Y}}_{\mathtt{LB}}^n(\boldsymbol{\mu}) = \Big\{ \boldsymbol{y} \in \boldsymbol{\mathcal{B}} \,\Big|\, \mathtt{I}(\boldsymbol{\mu}', \boldsymbol{y}) \geq \alpha_h(\boldsymbol{\mu}') \quad \forall \boldsymbol{\mu}' \in \mathbb{P}_{M_\alpha}(\boldsymbol{\mu}; \mathbb{C}_n), \\ \mathtt{I}(\boldsymbol{\mu}', \boldsymbol{y}) \geq \alpha_{\mathtt{LB}}^{n-1}(\boldsymbol{\mu}') \quad \forall \boldsymbol{\mu}' \in \mathbb{P}_{M_p}(\boldsymbol{\mu}; \Xi) \Big\}.$$

As a consequence, we have the property that

$$\boldsymbol{\mathcal{Y}}_{\mathtt{LB}}^1(\boldsymbol{\mu}) \subset \boldsymbol{\mathcal{Y}}_{\mathtt{LB}}^2(\boldsymbol{\mu}) \subset \cdots \subset \boldsymbol{\mathcal{Y}}_{\mathtt{LB}}^n(\boldsymbol{\mu}) \subset \cdots \subset \boldsymbol{\mathcal{Y}} \subset \cdots \subset \boldsymbol{\mathcal{Y}}_{\mathtt{UB}}^n \subset \cdots \subset \boldsymbol{\mathcal{Y}}_{\mathtt{UB}}^2 \subset \boldsymbol{\mathcal{Y}}_{\mathtt{UB}}^1.$$

Note that solving $\alpha_{\mathtt{LB}}^n(\boldsymbol{\mu}) = \min_{\boldsymbol{y} \in \boldsymbol{\mathcal{Y}}_{\mathtt{LB}}^n(\boldsymbol{\mu})} \mathtt{I}(\boldsymbol{\mu}, \boldsymbol{y})$ corresponds to a linear program (LP) of $\hat{Q}$ design variables and $2\hat{Q} + M_\alpha + M_p$ conditions. This is independent of $\mathcal{N}$.

Having defined the two sets $\boldsymbol{\mathcal{Y}}_{\mathtt{LB}}^n(\boldsymbol{\mu})$ and $\boldsymbol{\mathcal{Y}}_{\mathtt{UB}}^n$, we can define a greedy selection in order to enrich the space $\mathbb{C}_n$ and build $\mathbb{C}_{n+1}$ at all stages of $n$. The algorithm is defined as follows.

Given some error tolerance `Tol`, some initial set $\mathbb{C}_1 = \{\boldsymbol{\mu}_1\}$, and $n = 1$ do:

1. For each $\boldsymbol{\mu} \in \Xi$:
   a. Compute the upper bound $\alpha_{\mathtt{UB}}^n(\boldsymbol{\mu}) = \min_{\boldsymbol{y} \in \boldsymbol{\mathcal{Y}}_{\mathtt{UB}}^n} \mathtt{I}(\boldsymbol{\mu}, \boldsymbol{y})$.
   b. Compute the lower bound $\alpha_{\mathtt{LB}}^n(\boldsymbol{\mu}) = \min_{\boldsymbol{y} \in \boldsymbol{\mathcal{Y}}_{\mathtt{LB}}^n(\boldsymbol{\mu})} \mathtt{I}(\boldsymbol{\mu}, \boldsymbol{y})$.
   c. Define the error estimate $\eta(\boldsymbol{\mu}) = 1 - \frac{\alpha_{\mathtt{LB}}^n(\boldsymbol{\mu})}{\alpha_{\mathtt{UB}}^n(\boldsymbol{\mu})}$.
2. Select $\boldsymbol{\mu}_{n+1} = \mathrm{argmax}_{\boldsymbol{\mu} \in \boldsymbol{\mathcal{P}}} \eta(\boldsymbol{\mu})$ and set $\mathbb{C}_{n+1} = \mathbb{C}_n \cup \{\boldsymbol{\mu}_{n+1}\}$.
3. If $\max_{\boldsymbol{\mu} \in \boldsymbol{\mathcal{P}}} \eta(\boldsymbol{\mu}) \leq \mathtt{Tol}$, `stop`.
4. Solve the generalized eigenvalue problem (3.8) associated with $\boldsymbol{\mu}_{n+1}$ and store $\boldsymbol{y}^{n+1}$.
5. Set $n := n + 1$ and `goto 1`.

**3.3.2. Online procedure of SCM.** Once the offline procedure as described above is finished, we denote $\boldsymbol{\mathcal{Y}}_{\mathtt{LB}}^n(\boldsymbol{\mu})$ by $\boldsymbol{\mathcal{Y}}_{\mathtt{LB}}(\boldsymbol{\mu})$ and $\boldsymbol{\mathcal{Y}}_{\mathtt{UB}}^n$ by $\boldsymbol{\mathcal{Y}}_{\mathtt{UB}}$.

For any arbitrary parameter value $\boldsymbol{\mu} \in \boldsymbol{\mathcal{P}}$, we can then compute a lower bound $\alpha_{\mathtt{LB}}(\boldsymbol{\mu})$ by retaining only the information about $\alpha_h(\boldsymbol{\mu})$ for all $\boldsymbol{\mu} \in \mathbb{C}_n$ and $\alpha_{\mathtt{LB}}(\boldsymbol{\mu})$ for all $\boldsymbol{\mu} \in \Xi$: For any new $\boldsymbol{\mu} \in \boldsymbol{\mathcal{P}}$, find the solution of

$$\alpha_{\mathtt{LB}}(\boldsymbol{\mu}) = \min_{\boldsymbol{y} \in \boldsymbol{\mathcal{Y}}_{\mathtt{LB}}(\boldsymbol{\mu})} \mathtt{I}(\boldsymbol{\mu}, \boldsymbol{y}),$$

which again consists of an LP with $\hat{Q}$ design variables and $2\hat{Q} + M_\alpha + M_p$ constraints.

**3.3.3. Affine decomposition for complex matrices.** Here we discuss how the affine decomposition (3.5) of the square of the operator can be obtained. Based on the affine decomposition (2.11) we introduce the family of parameter-independent operators represented by matrices $\mathtt{A}_q : \boldsymbol{X}_h \mapsto \boldsymbol{X}_h$ such that $(\mathtt{A}_q \boldsymbol{v}_h, \boldsymbol{w}_h)_{\boldsymbol{X}_h} = a^q[\boldsymbol{v}_h, \boldsymbol{w}_h]$, and thus $\mathtt{A}(\boldsymbol{\mu}) = \sum_{q=1}^{Q_\mathtt{a}} \theta_\mathtt{a}^q(\boldsymbol{\mu})\, \mathtt{A}_q$. As a consequence,

$$\begin{aligned}\mathtt{A}^*\mathtt{A}(\boldsymbol{\mu}) &= \sum_{q,m=1}^{Q_\mathtt{a}} \overline{\theta_\mathtt{a}^m(\boldsymbol{\mu})}\theta_\mathtt{a}^q(\boldsymbol{\mu})\, \mathtt{A}_m^*\mathtt{A}_q \\ &= \sum_{q=1}^{Q_\mathtt{a}} \overline{\theta_\mathtt{a}^q(\boldsymbol{\mu})}\theta_\mathtt{a}^q(\boldsymbol{\mu})\, \mathtt{A}_q^*\mathtt{A}_q + \sum_{q=1}^{Q_\mathtt{a}} \sum_{m=q+1}^{Q_\mathtt{a}} \left[\overline{\theta_\mathtt{a}^m(\boldsymbol{\mu})}\theta_\mathtt{a}^q(\boldsymbol{\mu})\, \mathtt{A}_m^*\mathtt{A}_q + \overline{\theta_\mathtt{a}^q(\boldsymbol{\mu})}\theta_\mathtt{a}^m(\boldsymbol{\mu})\, \mathtt{A}_q^*\mathtt{A}_m\right].\end{aligned}$$

For the sake of short notation, denote $z_{mq} = \overline{\theta_\mathtt{a}^m(\boldsymbol{\mu})}\theta_\mathtt{a}^q(\boldsymbol{\mu})$ and observe that $z_{qm} = \overline{z_{mq}}$. Therefore

$$\begin{aligned}&z_{mq}\mathtt{A}_m^*\mathtt{A}_q + z_{qm}\mathtt{A}_q^*\mathtt{A}_m \\ &\qquad = z_{mq}\mathtt{A}_m^*\mathtt{A}_q + \overline{z_{mq}}\mathtt{A}_q^*\mathtt{A}_m \\ &\qquad = \Re(z_{mq})(\mathtt{A}_m^*\mathtt{A}_q + \mathtt{A}_q^*\mathtt{A}_m) + i\Im(z_{mq})(\mathtt{A}_m^*\mathtt{A}_q - \mathtt{A}_q^*\mathtt{A}_m) \\ &\qquad = \Re(z_{mq})(\mathtt{A}_m + \mathtt{A}_q)^*(\mathtt{A}_m + \mathtt{A}_q) + \Im(z_{mq})(\mathtt{A}_m + i\mathtt{A}_q)^*(\mathtt{A}_m + i\mathtt{A}_q) \\ &\qquad\quad - [\Re(z_{mq}) + \Im(z_{mq})]\, \mathtt{A}_q^*\mathtt{A}_q - [\Re(z_{mq}) + \Im(z_{mq})]\, \mathtt{A}_m^*\mathtt{A}_m,\end{aligned}$$

and thus

$$\begin{aligned}&\mathtt{A}^*\mathtt{A}(\boldsymbol{\mu}) \\ &= \sum_{q=1}^{Q_\mathtt{a}} \left[z_{qq} - \sum_{m=q+1}^{Q_\mathtt{a}} [\Re(z_{mq}) + \Im(z_{mq})]\right] \mathtt{A}_q^*\mathtt{A}_q - \sum_{q=1}^{Q_\mathtt{a}} \sum_{m=q+1}^{Q_\mathtt{a}} [\Re(z_{mq}) + \Im(z_{mq})]\, \mathtt{A}_m^*\mathtt{A}_m \\ &\qquad + \sum_{q=1}^{Q_\mathtt{a}} \sum_{m=q+1}^{Q_\mathtt{a}} \Re(z_{mq})(\mathtt{A}_m + \mathtt{A}_q)^*(\mathtt{A}_m + \mathtt{A}_q) + \Im(z_{mq})(\mathtt{A}_m + i\mathtt{A}_q)^*(\mathtt{A}_m + i\mathtt{A}_q) \\ &= \sum_{q=1}^{Q_\mathtt{a}} \left[z_{qq} - \sum_{m=1}^{q-1} [\Re(z_{qm}) - \Im(z_{qm})] - \sum_{m=q+1}^{Q_\mathtt{a}} [\Re(z_{mq}) + \Im(z_{mq})]\right] \mathtt{A}_q^*\mathtt{A}_q \\ &\qquad + \sum_{q=1}^{Q_\mathtt{a}} \sum_{m=q+1}^{Q_\mathtt{a}} \Re(z_{mq})(\mathtt{A}_m + \mathtt{A}_q)^*(\mathtt{A}_m + \mathtt{A}_q) + \Im(z_{mq})(\mathtt{A}_m + i\mathtt{A}_q)^*(\mathtt{A}_m + i\mathtt{A}_q),\end{aligned}$$

where the second equality follows from reordering the coefficients corresponding to the terms $\mathtt{A}_m^*\mathtt{A}_m$ and interchanging the indices $m$ and $q$. We are therefore able to write $\mathtt{A}^*\mathtt{A}$ as a linear combination of semipositive Hermitian matrices, i.e.,

$$\mathtt{A}^*\mathtt{A}(\boldsymbol{\mu}) = \sum_{\hat{q}=1}^{\hat{Q}} z_{\hat{q}}(\boldsymbol{\mu})\mathtt{Z}_{\hat{q}},$$

for $\hat{Q} = Q_\mathtt{a}^2$ and using an appropriate reindexing.

**4. Numerical results.** In the following we offer a number of tests to verify the above results and demonstrate the accuracy and efficiency of the overall framework. To keep things simple and consistent, we consider scattering examples based on the

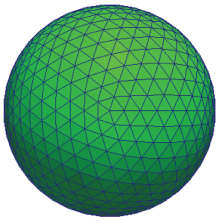

FIG. 1. *Coarse sphere.*

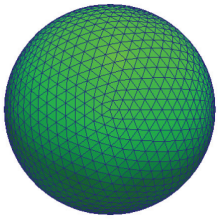

FIG. 2. *Fine sphere.*

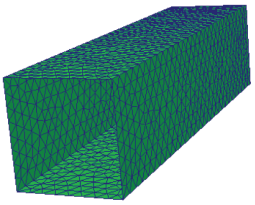

FIG. 3. *Cavity.*

shapes illustrated in Figures 1, 2, and 3 through their meshes. The computational workflow consists first of computing the affine decompositions (2.11)–(2.12) using the EIM as explained in [5], applying the SCM, and then assembling the reduced basis according to section 2.2. All these three parts are independent, and no synergies can be used.

**4.1. SCM.** We first test the SCM on its own, unrelated to the RBM.

**4.1.1. Influence of $M_\alpha$ and $M_p$.** The first set of tests consists of analyzing the dependence of the convergence on $M_\alpha$ and $M_p$. Higher values of those two numbers imply more work for evaluating the lower bound of the inf-sup constant, playing an important role during the online stage of the RBM. The convergence of the SCM is, however, expected to be faster than for smaller values.

To analyze the dependence on the convergence of the SCM we consider the sphere discretized as illustrated in Figure 1 and a range of wave-numbers $k \in \boldsymbol{\mathcal{P}_a} = [1, 3]$. A set of 501 equidistant points in the interval $\boldsymbol{\mathcal{P}_a} = [1, 3]$ is used as trial set $\Xi$. The profile of the inf-sup constant is presented in Figure 4. Note the presence of the first interior resonant wave-number at $k_1 = 2.743$. Figure 5 shows the convergence of the error quantity (3.7) for varying $M = M_p = M_\alpha = 5, 10, 15, 20, 25$, and Figures 6 and 7 show the convergence of (3.7) for fixed $M_p = 15$ (resp., $M_\alpha = 15$) and $M_\alpha = 5, 10, 15, 20, 25$ (resp., $M_p = 5, 10, 15, 20, 25$). We notice that for this example it is required that $M_\alpha > 10$ for a proper convergence, and it seems that $M_p$ does not have a major influence in this particular example on the convergence rate.

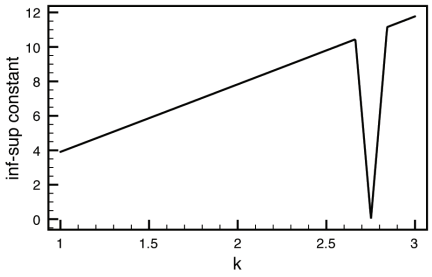


FIG. 4. *Profile of the inf-sup constant for* $k \in [1, 3]$.

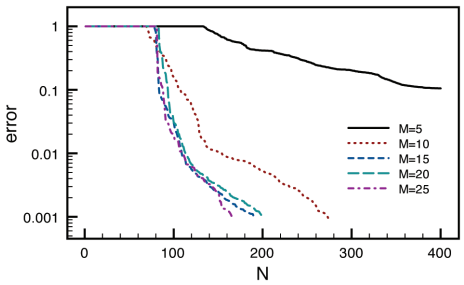


FIG. 5. *Convergence behavior of the SCM under variation of* $M = M_\alpha = M_p = 5, 10, 15, 20, 25$.

A physically more interesting case is to increase the interval of wave-numbers under consideration. We now consider $k \in \boldsymbol{\mathcal{P}_a} = [1, 5]$, which requires the use of a finer discretization of the sphere (cf. Figure 2) to guarantee 10 degrees of freedom per

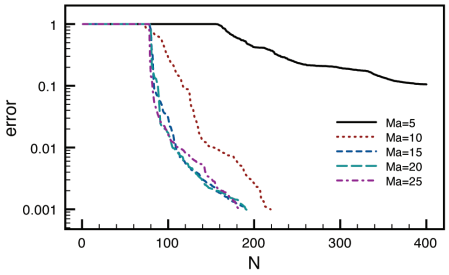


FIG. 6. *Convergence behavior of the SCM under variation of* $M_\alpha = 5, 10, 15, 20, 25$ *for a fixed* $M_p = 15$.

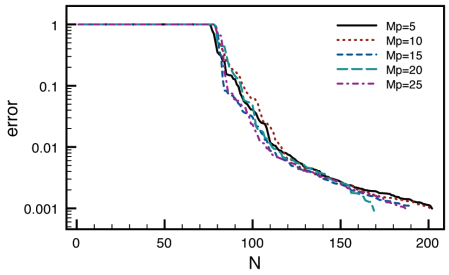


FIG. 7. *Convergence behavior of the SCM under variation of* $M_p = 5, 10, 15, 20, 25$ *for a fixed* $M_\alpha = 15$.

wavelength. A set of 501 equidistant points in the interval $\mathcal{P}_a = [1, 5]$ is used as trial set $\Xi$.

The parameters of the SCM are set to $\texttt{Tol} = 0.1$, $M_\alpha = M_p = 20$, and Figure 8 shows the convergence of the SCM, measured by (3.7), in this case. Figure 9 plots the lower and the upper bound of the inf-sup constant and the parameter values that were chosen during the greedy algorithm. One can observe that the resonant wave-numbers $k_1 = 2.743$, $k_2 = 3.870$, $k_3 = 4.493$, and $k_4 = 4.973$ (cf. [1, Table 6.1]) are causing the inf-sup constant to be (close to) zero.

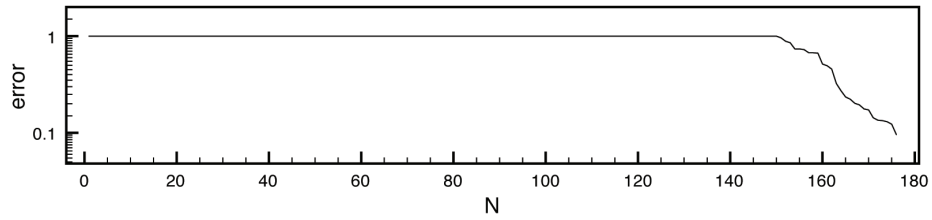


FIG. 8. *Convergence of the SCM for* $k \in [1, 5]$ *using a sphere as geometry (Figure 2) and* $\texttt{Tol} = 0.1$, $M_\alpha = M_p = 20$.

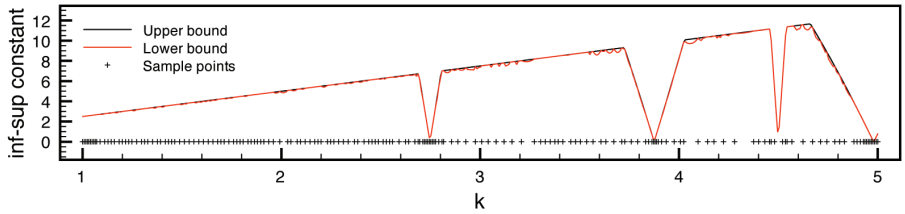


FIG. 9. *The lower and the upper bound of the inf-sup constant for* $k \in [1, 5]$ *using a sphere as geometry (Figure 2) and* $\texttt{Tol} = 0.1$, $M_\alpha = M_p = 20$. *In addition, the chosen parameter values by the SCM are indicated.*

We finally consider the cavity illustrated in Figure 3 for a range of wave-numbers $k \in \mathcal{P}_a = [10, 20]$, $\texttt{Tol} = 10^{-3}$, and $M_\alpha = M_p = 20$. A point set of 1001 equidistant points in $\mathcal{P}_a = [10, 20]$ is chosen to build the trial set $\Xi$. The corresponding convergence of the SCM is presented in Figure 10, and the lower and the upper bound

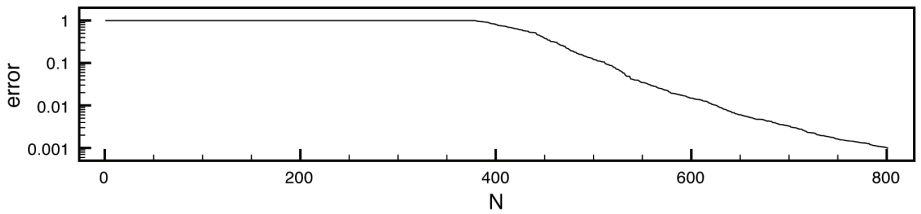


FIG. 10. *Convergence of the SCM for* $k \in [10, 20]$ *using the cavity (Figure* 3*) as geometry and* $\texttt{Tol} = 10^{-3}$, $M_\alpha = M_p = 20$.

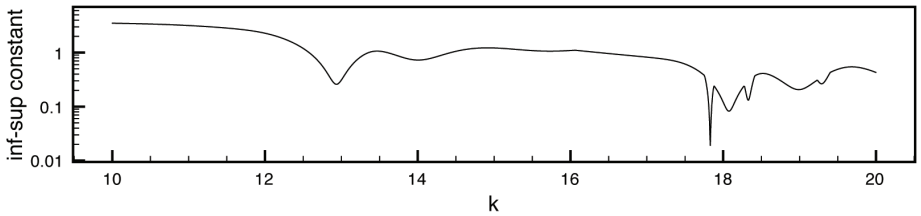


FIG. 11. *The lower and the upper bound (indistinguishable) of the inf-sup constant for* $k \in [10, 20]$ *using the cavity (Figure* 3*) as geometry and* $\texttt{Tol} = 10^{-3}$, $M_\alpha = M_p = 20$.

(indistinguishable) of the inf-sup constant are illustrated in Figure 11. One can observe the various "negative peaks" where the inf-sup constant drops locally due to near-resonances. We notice that the constant varies two orders of magnitude, which may have an essential impact on the a posteriori estimates of the RBM.

**4.2. Certified RBM.** In this section, we present numerical results for the full certified RBM, which relies on the SCM in order to provide accurate a posteriori estimates.

We first consider the problem associated with the sphere presented in Figure 2 and an interval of wave-numbers $k \in \boldsymbol{\mathcal{P}} = [4.52, 4.95]$. Since $\boldsymbol{\mathcal{P}} = \boldsymbol{\mathcal{P}}_{\boldsymbol{a}} = [4.52, 4.95]$ in this case, the same trial set $\Xi$ consisting of 501 equidistant points is used for both the SCM and the greedy algorithm of the RBM.

As indicated in Figure 9 the EFIE is not well-posed at the resonant wave-numbers which need to be excluded. Figure 12 shows the convergence of the maximal error (over the parameter space and measured in the $H(\mathrm{div}, \Omega)$-norm) and the residual-based error estimation $\eta_N$, which, as described in Proposition 3.1, is an upper bound of the error. The error profile during the last iteration ($N = 4$) of the greedy algorithm of the RBM is illustrated in Figure 13 as well as the chosen parameter values.

Further, we reconsider the example using the cavity (Figure 3) as geometry and having parameters $k \in \boldsymbol{\mathcal{P}} = \boldsymbol{\mathcal{P}}_{\boldsymbol{a}} = [10, 20]$ for

$$\hat{\boldsymbol{d}} = -(\sin(\pi/2), 0, \cos(\pi/2)) \qquad \text{and} \qquad \hat{\boldsymbol{d}}_0 = (\sin(\pi/2), 0, \cos(\pi/2)),$$

so that we are considering the backscattering (monostatic) RCS. Again, the same trial set $\Xi$ consisting of 1001 equidistant points is used for both the SCM and the greedy algorithm of the RBM. The polarization is set to $\hat{\boldsymbol{p}} = \frac{1}{\sqrt{2}}(1, 0, -1)$. Observe that the only active parameter here is the wave-number $k$. In Figure 14 we plot the convergence of the residual a posteriori estimate and the corresponding error measured in the $\boldsymbol{H}(\mathrm{div})$-norm. Figure 15 illustrates the error profile over the parameter space

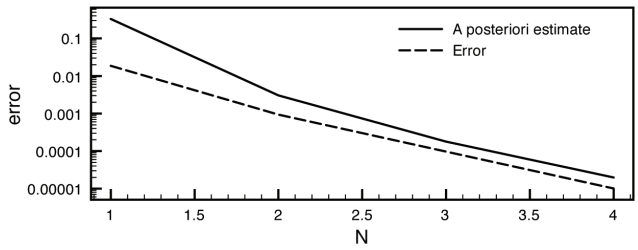


FIG. 12. *Maximal error and a posteriori error estimation over the parameter space at each step of the greedy algorithm during the reduced basis assembling process for a sphere as in Figure 2 with* $k \in [4.52, 4.95]$.

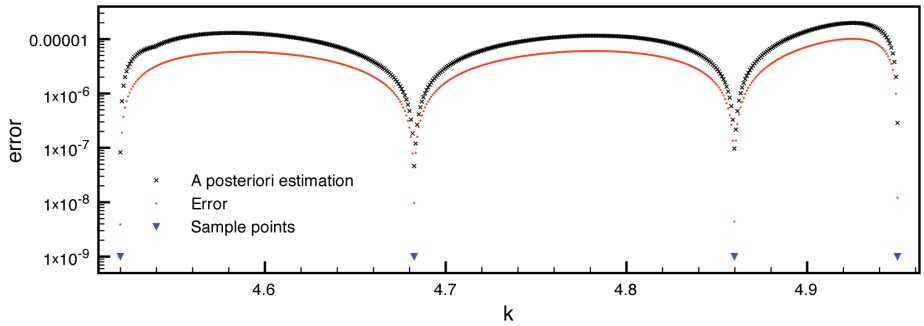


FIG. 13. *Error profile over the parameter space at the last iteration of the greedy algorithm during the reduced basis assembling process for a sphere as in Figure 2 with* $k \in [4.52, 4.95]$.

at the last iteration ($N = 23$) and for $N = 16$, whereas Figure 16 shows the efficiency index

$$\text{eff}(\boldsymbol{\mu}) = \frac{\eta(\boldsymbol{\mu})}{\|\boldsymbol{u}_h(\boldsymbol{\mu}) - \boldsymbol{u}_N(\boldsymbol{\mu})\|_{\boldsymbol{X}_h}}$$

depending on $\boldsymbol{\mu} \in \boldsymbol{\mathcal{P}}$ for three different values of $N$. We observe that the a posteriori estimate $\eta_N$ is indeed an upper bound of the error (in the $H(\text{div}, \Omega)$-norm) as indicated by Proposition 3.1 except close to parameter values that are chosen during the sampling strategy. At such points, the error and the error estimate are very small (even theoretically equal to zero at the sample points); in practical computations rounding errors, however, dominate. This may lead to the efficiency index being smaller than one.

Figure 17 illustrates the RCS signal for values $k \in [10, 20]$ based on the reduced basis approximation and the truth solver (the BEM), including the upper and lower error bars according to Proposition 3.5 for $N = 21$, $N = 22$, and at the final iteration $N = 23$.

Finally, in Figure 18 the error in the RCS (compared to the RCS computed with the truth solver, which is the BEM in our case) and the certified error bound are shown. We observe that the error estimate certifies the error well and that the estimation is in general pessimistic.

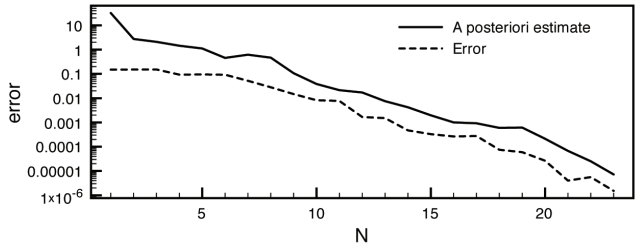


FIG. 14. *Maximal error and a posteriori error estimation over the parameter space at each step of the greedy algorithm during the reduced basis assembling process for a cavity as in Figure* 3 *with* $k \in [10, 20]$.

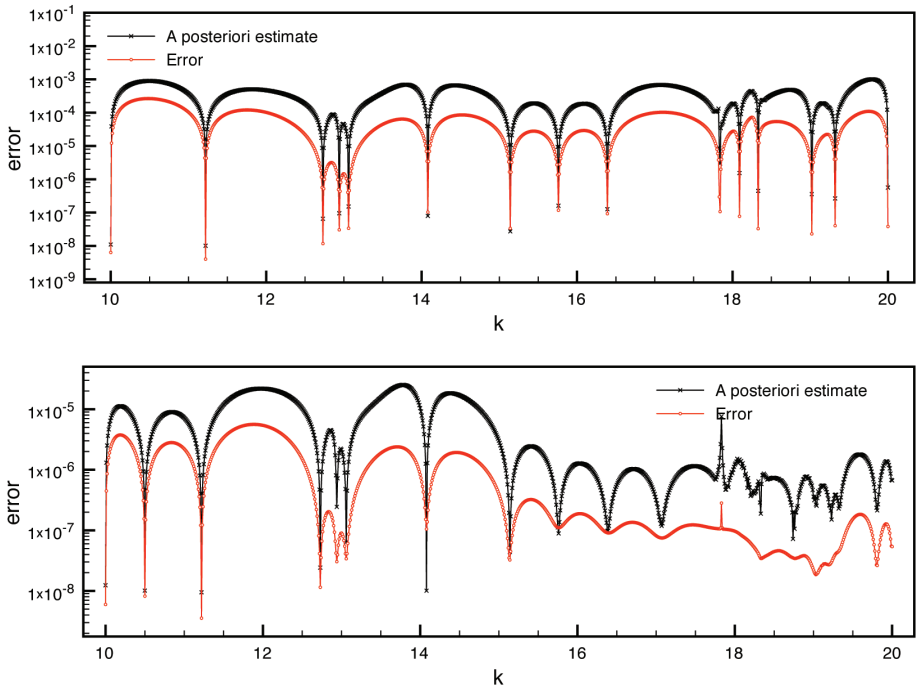


FIG. 15. *Error profile over the parameter space at iterations* $N = 16$ *(top) and* $N = 23$ *(bottom) of the greedy algorithm during the reduced basis assembling process for a cavity as in Figure* 3 *with* $k \in [10, 20]$.

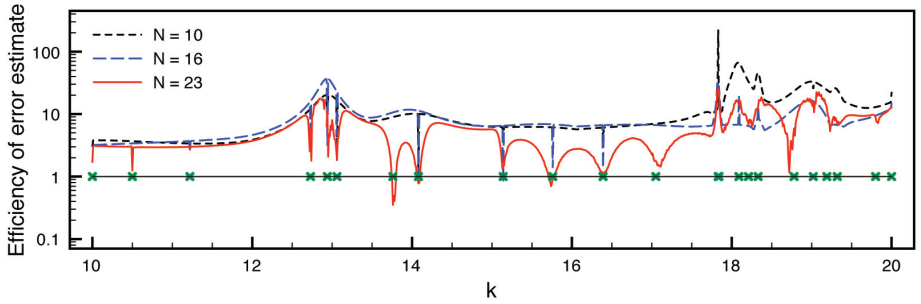


FIG. 16. *Efficiency of the error estimator over the parameter space for* $N = 10, 16, 23$ *during the greedy algorithm for the reduced basis assembling process for a cavity as in Figure* 3 *with* $k \in [10, 20]$ *and the sampling points for* $N = 23$.

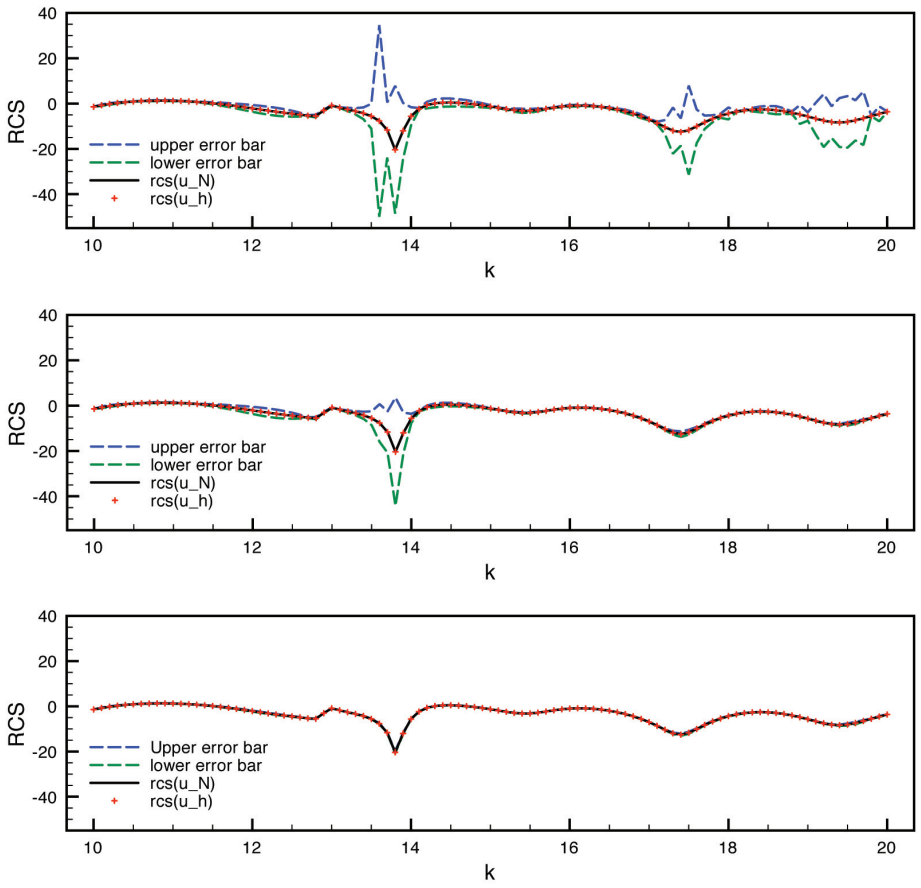


FIG. 17. *The RCS for* $k \in [10, 20]$ *using the reduced basis approximation and the BEM including error bars for* $N = 21$ *(top),* $N = 22$ *(middle), and* $N = 23$ *(bottom).*

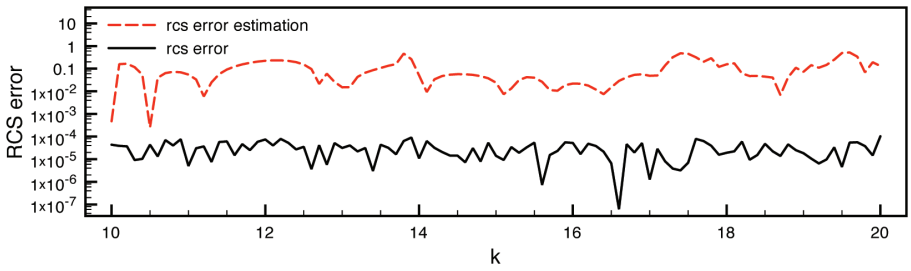


FIG. 18. *The error of the RCS for* $k \in [10, 20]$ *using the reduced basis approximation and the certified error estimation for the RCS at the final iteration* $N = 23$.

**5. Concluding remarks.** In the present work we have developed a complete framework for the certified reduced basis method (RBM) applied to the parameterized electric field integral equation (EFIE). The parameters consist of the wave-number, the angle, and the polarization of the incident plane wave.

We presented in detail how the rigorous a posteriori estimates, which are key ingredients in certifying the error tolerance of the model reduction, are developed in the present case. An important feature is to give an estimate of the parameter-dependent inf-sup constant by means of the successive constraint method (SCM). One particularity of the EFIE is that the SCM needed to be generalized to complex matrices. Further, we derived error estimates that certify the error of the radar cross section (RCS), which is a nonlinear functional of the unknowns of the EFIE. Finally, we presented some numerical examples to test the performance of the SCM and the RBM. Future work includes generalizing the method to the combined field integral equation (CFIE), which is more frequently used in practice due to better stability properties.

## REFERENCES

[1] J. H. BRAMBLE, T. V. KOLEV, AND J. E. PASCIAK, *The approximation of the Maxwell eigenvalue problem using a least-squares method*, Math. Comp., 74 (2005) pp. 1575–1598.
[2] A. BUFFA AND S. H. CHRISTIANSEN, *The electric field integral equation on Lipschitz screens: Definitions and numerical approximation*, Numer. Math., 94 (2003), pp. 229–267.
[3] Y. CHEN, J. S. HESTHAVEN, Y. MADAY, AND J. RODRIGUEZ, *Improved successive constraint method based a posteriori error estimate for reduced basis approximation of* 2*d Maxwell's problem*, M2AN Math. Model. Numer. Anal., 43 (2009), pp. 1099–1116.
[4] Y. CHEN, J. S. HESTHAVEN, Y. MADAY, AND J. RODRÍGUEZ, *Certified reduced basis methods and output bounds for the harmonic Maxwell's equations*, SIAM J. Sci. Comput., 32 (2010), pp. 970–996.
[5] B. FARES, J. S. HESTHAVEN, Y. MADAY, AND B. STAMM, *The reduced basis method for the electric field integral equation*, J. Comput. Phys., 230 (2011), pp. 5532–5555.
[6] R. HARRINGTON, *Field Computation by Moment Methods*, Macmillan, New York, 1968.
[7] R. HIPTMAIR AND C. SCHWAB, *Natural boundary element methods for the electric field integral equation on polyhedra*, SIAM J. Numer. Anal., 40 (2002), pp. 66–86.
[8] D. B. P. HUYNH, G. ROZZA, S. SEN, AND A. T. PATERA, *A successive constraint linear optimization method for lower bounds of parametric coercivity and inf-sup stability constants*, C. R. Math. Acad. Sci. Paris, 345 (2007), pp. 473–478.
[9] D. B. P. HUYNH, D. J. KNEZEVIC, Y. CHEN, J. S. HESTHAVEN, AND A. T. PATERA, *A natural-norm successive constraint method for inf-sup lower bounds*, Comput. Methods Appl. Mech. Engrg., 199 (2010), pp. 1963–1975.
[10] A. T. PATERA AND G. ROZZA, *Reduced Basis Approximation and A Posteriori Error Estimation for Parametrized Partial Differential Equations*, Version 1.0, MIT, Cambridge, MA, 2006,

(tentative rubric) MIT Pappalardo Graduate Monographs in Mechanical Engineering, to appear.

[11] P.-A. Raviart and J. M. Thomas, *A mixed finite element method for 2nd order elliptic problems*, in Mathematical Aspects of Finite Element Methods, Lecture Notes in Math. 606, Springer, Berlin, 1977, pp. 292–315.

[12] G. Rozza, D. B. P. Huynh, and A. T. Patera, *Reduced basis approximation and a posteriori error estimation for affinely parametrized elliptic coercive partial differential equations: Application to transport and continuum mechanics*, Arch. Comput. Methods Eng., 15 (2008), pp. 229–275.

[13] S. A. Sauter and C. Schwab, *Boundary Element Methods*, Springer Ser. Comput. Math. 39, Springer, Berlin, 2011.